An-Najah National University
Faculty of Graduate Studies

STUDY THE ACTIVE-CARBON (AC)/CARBON-NANOFIBERS (CNF_S) AS SUPERCAPACITOR ELECTRODES USING DIFFERENT AQUEOUS ELECTROLYTES (6 M KOH, 1 M H_2SO_4, AND DIFFERENT CONCENTRATIONS OF DEAD SEA WATER)

By
Kholoud Waleed Bourini

Supervisors
Dr. Allan Daraghmeh
Dr. Iyad Saadeddin

This Thesis is Submitted in Partial Fulfillment of the Requirements for the Degree of Master of Physics, Faculty of Graduate Studies, An-Najah National University, Nablus - Palestine.

2024

STUDY THE ACTIVE-CARBON (AC)/CARBON-NANOFIBERS (CNF_S) AS SUPERCAPACITOR ELECTRODES USING DIFFERENT AQUEOUS ELECTROLYTES (6 M KOH, 1 M H_2SO_4, AND DIFFERENT CONCENTRATIONS OF DEAD SEA WATER)

By
Kholoud Waleed Bourini

This Thesis was defended successfully on 09/03/2024 and approved by:

Dr. Allan Daraghmeh	
Supervisor	Signature
Dr. Iyad Saadeddin	
Co-Supervisor	Signature
Dr. Muayad Abu Saa	
External Examiner	Signature
Prof. Sami Jaber	
Internal Examiner	Signature

Dedication

This work is dedicated to my family, especially my father and mother, for always supporting and encouraging me. Without their guidance and assistance, I wouldn't have been able to achieve my current goals. They have always believed in my abilities and provided me with the necessary support to overcome difficulties. I'm grateful for their unwavering backing, even during challenging times.

Finally, I would also like to dedicate this work to my children, Rodaina, Lian, Youssef, and Mohammed, to express my love and to pray that it will inspire them to strive for excellence in everything they do.

Acknowledgements

First of all, I thank and praise God for facilitating the path of knowledge for me and granting me the ability to complete this study. I raise my hands in prayer to Him, hoping for continued success. Then I extend my thanks, appreciation, and gratitude to my supervisor, Dr. Allan Daraghmeh, for his advice, guidance, and inspiration to complete this study and produce it in the best possible way, and I’m extremely grateful to the physics and chemistry laboratories for their assistance.

Special thanks to Barcelona University, Dr. Shahzad Hussain, Dr. Lorance Servera, and Dr. Albert Cirera for their time and effort to complete this research. I am grateful to the university's Faculty of Postgraduate Studies, under the direction of Dr. Kefah Barham, for their ongoing assistance. My deepest gratitude goes out to the discussion committee members, the external examiner, Dr. Muayad Abu Saa, and the internal examiner, Prof. Sami Jaber, for their thoughtful observations and insightful criticisms during the session.

Finally, I would like to express my gratitude to everyone who helped me do this assignment without any hesitation. This thesis would not have been feasible without their assistance.

Declaration

I, the undersigned, declare that I submitted the thesis entitled:

STUDY THE ACTIVE-CARBON (AC)/CARBON-NANOFIBERS (CNF_S) AS SUPERCAPACITOR ELECTRODES USING DIFFERENT AQUEOUS ELECTROLYTES (6 M KOH, 1 M H_2SO_4, AND DIFFERENT CONCENTRATIONS OF DEAD SEA WATER)

I declare that the work provided in this thesis, unless otherwise referenced, is the researcher's own work, and has not been submitted elsewhere for any other degree or qualification.

Student's Name Kholoud Waleed Bourini

Signature: 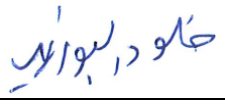

Date: 09/03/2024

List of Contents

List of Tables

List of Figures

List of Appendices

STUDY THE ACTIVE-CARBON (AC)/CARBON-NANOFIBERS (CNF_S) AS SUPERCAPACITOR ELECTRODES USING DIFFERENT AQUEOUS ELECTROLYTES (6 M KOH, 1 M H_2SO_4, AND DIFFERENT CONCENTRATIONS OF DEAD SEA WATER)

By
Kholoud Waleed Bourini
Supervisors
Dr. Allan Daraghmeh
Dr. Iyad Saadeddin

Abstract

This thesis explores the effects of varying electrolyte compositions on a composite AC/CNFs electrode, consisting of 90% activated carbon (AC) and 10% carbon nanofibers (CNFs), designed for supercapacitors. Four different electrolytes were employed: 6 M potassium hydroxide (KOH), 1 M sulfuric acid (H_2SO_4), Dead Sea water, and concentrated Dead Sea water. The electrode's electrochemical properties were analyzed using cyclic voltammetry (CV), galvanostatic charge-discharge (GCD), and electrochemical impedance spectroscopy (EIS).

In CV tests conducted at a 100 mV/s scan rate, the electrodes exhibited specific capacitances (Cs) close to each other with values at 78.50 F/g for H_2SO_4, 77.40 F/g for KOH, and 78.54 F/g for Dead Sea water. However, the electrode with concentrated Dead Sea water recorded a lower Cs of 56.54 F/g. At a lower scan rate of 5 mV/s, the Cs increased, with KOH showing the highest capacitance of 157.86 F/g, while the other electrolytes recorded slightly lower values.

GCD studies indicated a decrease in Cs with higher current densities. At a low current density of 0.4 A/g, concentrated Dead Sea water electrolyte showed the highest Cs of 84.40 F/g, contrasting with the lowest Cs of 52.40 F/g for the KOH electrolyte. Other electrolytes exhibited similar capacitance around 81 F/g at this current density. The stability tests confirmed that all electrodes maintained their performance over numerous cycles, highlighting their potential for long-term supercapacitor applications.

EIS measurements revealed that the electrodes with 1 M H_2SO_4 showed the highest specific capacitance of 150.3 F/g. The concentrated Dead Sea water electrolyte exhibited the fastest charge transfer, indicated by the highest knee frequency at 0.125 Hz. The

electrode with regular Dead Sea water displayed the lowest time constant, suggesting quicker charging and discharging capabilities. Impedance values and phase angles further confirmed diverse capacitive behaviors across the electrolytes, with the regular Dead Sea water electrode showing characteristics closest to ideal capacitive behavior.

Surface examination of the AC/CNFs electrode revealed a coarse and porous structure, predominantly narrow, slit-like micropores, with a total pore volume of 0.693 cm^3/g and a specific surface area of 962.06 m^2/g. These physical attributes are crucial for the electrode's performance in supercapacitors.

Keywords: Active Carbon (AC), Carbon Nanofibers (CNFs), Supercapacitor Electrodes, Aqueous Electrolytes, Dead Sea Water.

Chapter One

Introduction

1.1 Overview

Supercapacitors (SCs) have caught the interest of the scientists due to their ability to provide energy storage and supply in systems that demand high energy production, such as fully electric cars. SCs are electrochemical capacitors with a remarkable energy density, approximately 100 times higher than that of conventional capacitors. Unlike batteries, which exhibit a high energy density but a low power density, supercapacitors have a more energy density and a considerably higher power density (1). The Ragone diagram Figure 1.1, which represents the energy density in relation to the power density for various electrical energy storage devices, evidences the unique position of supercapacitors or ultracapacitors compared to conventional fuel cells, batteries and dielectric capacitors. Fuel cells and batteries tend to mainly exhibit high energy density, while traditional dielectric capacitors are characterized by having a high power density. In this graph, supercapacitors reduce the gap between conventional capacitors and batteries, thus occupying an intermediate position as they efficiently combine energy and power high density (2). SCs have long life cycles and allow rapid charging and discharging of electrical energy due to the absence of chemical reactions in their operation. In addition, they are noted for their simple operating mechanism and efficient construction methods, as well as the low-cost materials. These devices are known as double-layer electric capacitors (EDLC) or ultracapacitors (1).

Figure 1.1

Ragone graph for different electrical energy storage devices

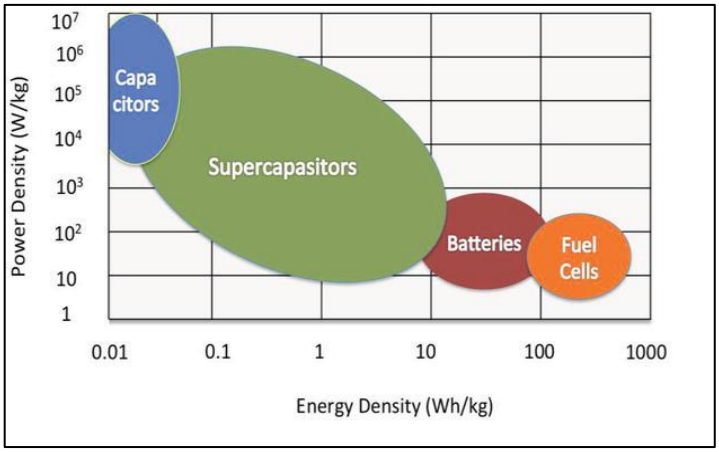

Note: Aslani M. Electrochemical double layer capacitors (supercapacitors). Standford University. 2012.

Electrode materials and the addition of electrolyte material between the electrodes distinguish supercapacitors from conventional capacitors. In SCs, materials with high porosity, which provide a high surface area, are used as electrodes to store more electrical charges inside the pores. A separating membrane moistened with ionic electrolyte is used to separate the two SCs electrodes instead of the dielectric material used in conventional capacitors. Fig. 1.2 in Appendix A presents the construction of the supercapacitor, that consist of two porous electrodes, a separating membrane and an electrolytic medium which can be solid or aqueous (3).

Supercapacitors are divided into three categories according to their various energy storage mechanisms. The first type is the double-layer electric capacitor (EDLC), where capacitance is achieved by the accumulation of a pure electrostatic charge at the electrode/electrolyte interface. By applying voltage to the plates, an opposite charge accumulates on both sides of the separator at the electrode-electrolyte interface, thus forming an electrical double layer, as illustrated in Figure 1.3 in Appendix A. The second type is the pseudocapacitor, which undergoes a rapid and reversible faradic process due to electrosorption, reduction-oxidation reactions and intercalation processes (5).

Unlike electric double-layer capacitors (EDLC), which store charge electrostatically, pseudocapacitors achieve charge storage by facilitating the transfer of charge between the electrode and the electrolyte. This approach gives pseudo capacitors a potential to achieve higher capacitance characteristics and energy densities compared to EDLCs (7). The third group is hybrids that combine the properties of EDLC and pseudo-capacitors in order to maximize the specific capacitance (Cs), which means the use of electrostatic and electrochemical mechanisms to store energy (8).

The specific capacitance (Cs) and the equivalent series resistance (ESR) are electrochemical characteristics of SCs that are controlled by electrode and electrolyte properties. These properties include pore size distribution, electrode specific surface area (SSA), electrode conductivity, electrode thickness, and ion mobility in the electrolyte (7).

Carbon materials are commonly employed as electrodes because they are affordable, available in various morphologies, and exhibit strong chemical and thermal properties (9). Porous carbon materials find extensive application in supercapacitors, particularly in

double-layer supercapacitors. This is because they possess a large specific surface area, very good electrical conductivity, and exceptional stability when exposed to various electrolytes across a broad spectrum of potentials and temperatures (10).

The tubular morphology of carbon nanofibers (CNFs) at the nanoscale provides a distinctive blend of excellent electrical conductivity and significant porosity within an easily accessible structure (11). Activated carbon (AC) is also a highly appealing material for supercapacitors due to its availability, low cost, exceptional porosity, strong stability, and effective charge-discharge cycling capabilities (12). The measured equivalent series resistance (ESR) values were quite different between CNFs (0.28 Ω) and AC (3.72 Ω). Additionally, CNFs demonstrated a superior specific power performance (1860 W/kg) compared to AC (450 W/kg). Conversely, it was observed that AC exhibited a higher specific energy, reaching 18.1 Wh/kg, compared to carbon nanofibers (CNFs) that registered 2 Wh/kg. This finding suggests that AC is more suitable for energy-related applications, while CNFs excel in power-related applications due to their lower ESR. The increase in the AC surface area contributes to a higher specific capacitance and, therefore, to a higher energy density. On the other hand, the lower ESR of CNFs is responsible for their higher power density. CNFs and AC supercapacitors exhibited remarkable stability for up to 2500 charge and discharge cycles (13). Therefore, composite electrodes containing more than one carbon form are developed to achieve the best characteristics that give high specific energy accompanied by a high-power density (14).

To preserve the integrity of electrodes (AC or CNFs) for supercapacitors, polymers' binders such as Polytetrafluoroethylene (PTFE), polyvynilidene chloride (PVDC) and polyvynilidene fluoride (PVDF) must be added in amounts ranging from 5 to 10 wt.%. However, binders block part of the carbon porosity and hence increase the electrical resistance of the electrodes (15, 16).

The capacity of the electrodes of supercapacitors to tolerate charges is specified by the materials of both the electrode and the electrolyte, giving the electrolyte material an importance comparable to that of the electrode material. The achievable voltage in a supercapacitor cell is determined through the breakdown voltage of the electrolyte, so the accessible energy density (which depends on the voltage) is finite by the electrolyte.

Likewise, the power density is subject to (ESR) of the cell, a parameter that is highly depends on the electrolytic conductivity (17).

Electrolytes are classified into two categories depending on their dissolving substance, organic and aqueous electrolytes. Aqueous electrolytes, which are water-based, are cheap, environmentally friendly, and have a significantly higher conductivity than non-aqueous electrolytes, lead to a higher power density (18, 19).

The electrolyte is a crucial and fundamental component of a supercapacitor, as it has a vital function in facilitating the transferal and balance charges between the positive and negative electrodes (20).

The interaction between electrodes and electrolytes in electrochemical processes has a significant impact on the state of the electrode-electrolyte interface and the internal structure of active materials. Therefore, the characteristics of the electrolyte-solution system play a crucial role in determining the electrochemical performance of supercapacitor devices. An appropriate electrolyte is essential to achieve a high energy density, a high power density and a long service life in supercapacitors. Figure 1.4 in Appendix A displays the commonly utilized electrolytes in supercapacitors. However, it's worth noting that there is currently no ideal electrolyte that fulfills all requests of electrochemical devices (21).

The majority of attempts focused on developing reliable and high-performance electrode materials using various electrode materials, new synthesis methods, various electrolyte types, etc. In addition, high-conductivity materials create a low-resistance pathway for ions to pass through the pores. Materials of excellent stability are also needed to determine the range of resistance of a material to erosion at higher operating voltages. The material underlying these characteristics implies that the supercapacitor will have a long service life (7).

1.2 Objectives of this work

The main goals of this study are:

1. Exploring the properties of nanocomposite AC/CNF electrodes, when they are utilized as supercapacitor electrodes.
2. Investigating the performance of previously prepared optimized nanocomposite AC/CNF supercapacitor electrodes under different aqueous electrolytes, separation membranes, and operating voltages.
3. Selecting the best aqueous electrolyte for such composite electrode (AC/CNF).
4. Analyzing the electrochemical characterization of the specific capacitance, the equivalent series resistance and the self-discharge of the prototype.

In addition to the main objectives, the study findings are hoped to enhance research on the characteristics of the supercapacitor, such as improving the specific capacitance, reducing the self-discharge rate, and increasing the amount of energy stored by weight unit.

1.3 Research questions and identified problems

The main issues covered by this thesis are:

1. What are the properties of nanocomposite AC/CNF electrodes when they are utilized as supercapacitor electrodes?
2. What are the best conditions of aqueous electrolyte, separation membrane, and operating voltage to achieve the best performance of previously prepared optimized Nano-composite AC/CNF supercapacitor electrodes?
3. What is the best aqueous electrolyte for such composite electrode (AC/CNF).

Chapter Two

Background and Literature review

2.1 Supercapacitors

2.1.1 Fundamentals of supercapacitors

In 1950, the design of a double electrochemical layer was proposed, and the operating principle of the supercapacitor was articulated. After that, different models such as the Helmholtz model, the Grahame model, the Gouy-Chapman model, and the Gouy-Chapman-Stern model were outlined, which were interested in the performance of electrodes under potentiostatic control in the electrolyte. Supercapacitors possess an exceptionally elevated energy density compared with conventional capacitors, usually many times of intensity greater than a large-capacity electrolytic capacitor (22).

Supercapacitors, also named as double-layer electric capacitors, double-layer electrochemical capacitors (EDLC), or ultra-capacitors, have garnered significant attention because of their enhanced electrochemical capabilities, extended operational lifespan, outstanding specific power, and rapid charge-discharge capabilities. While their energy density is similar to batteries, supercapacitors excel in terms of power density and cycling durability, surpassing batteries by several-fold. This positions them as a versatile and highly promising energy storage option, given the utilization of suitable and efficient materials (23).

Supercapacitors operate without relying on redox reactions, making the conventional terms "anode" and "cathode" somewhat inappropriate, although they are still commonly used. Instead, they create electric double layers (EDLs) at the interface between the electrolyte and the electrode, which store and release energy. This results in simultaneous electron movement through the external circuit, effectively delivering energy see Fig. 2.1 in Appendix A (24).

Supercapacitors currently manufactured for commercial use predominantly employ porous carbon materials featuring extensive surface areas and noble metal oxide systems. These commercial supercapacitors find widespread applications as energy sources for actuator devices, components for durable continuous circuits, mobile phones, and backup power supplies for RAM devices (25).

Batteries typically have a lower power capacity compared with conventional capacitors, which have high power densities but exhibit low energy densities. In contrast, supercapacitors manage to combine both a high power and energy density, and have long life cycles attributable to the absence of significant chemical reactions (26).

There are three main categories of supercapacitors that are classified according to their charge storage mechanism. Double-layer electrical capacitors (EDLCs) store electrical charge by forming an electrostatic double layer on their electrodes. On the other hand, pseudocapacitors (PCs) have the ability to store charge in a faradaic way through redox reactions on the electrode surface. In addition, hybrid supercapacitors combine the ability to store charge both faradaically and non-faradaically (27). Classification of the different types of supercapacitors is illustrated in Fig. 2.2 in Appendix A.

A comparison between the specifications of different types of supercapacitors is in Table 2.1.

Table 2.1

Supercapacitors' specifications

Parameters	EDLCs	Pseudo-capacitors	Hybrid SCs
Storage mechanism	Non-Faradaically	Faradaically	Faradaic and Non-Faradaic behavior
Specific capacitance	Low	High	High
Energy density	Low	High	High
Cyclic stability	High	Low	High
Material	Carbon materials such as activated carbon, carbon nanotubes, reduced graphene, etc.	Conductive polymers, metal oxygen/ sulfides/ metal phosphates and oxides, e.g. NiO, ZnO, PANI, MgO, etc.	Metal oxide/ carbon-based materials, conducting polymers/ carbon based materials, Metal organic framework/ carbon-based materials.

Note: Iqbal MZ, Aziz U. Supercapattery: Merging of battery-supercapacitor electrodes for hybrid energy storage devices. Journal of Energy Storage. 2022;46:103823.

2.1.2 The basic principle of Supercapacitors

A supercapacitor includes two electrodes arranged in parallel, separated by a non-conductive material containing an electrolyte between them, as illustrated in Figure 2.3 in Appendix A. When a voltage is operated upon electrodes, ions in the electrolyte are attracted to the electrode with the opposite charge, which leads to the formation of an electrostatic double layer (EDL) on each electrode, which arises from the accumulation of charge and its interaction with the surface of the electrode (29).

The two main storage principles of supercapacitor theory are (30):

1. In a double-layer capacitor, the accumulation of electrostatic charge is achieved by charge distribution in a Helmholtz double layer at the interface between the surface of a conductive electrode and an electrolyte. Charge separation occurs in a range of a few angstroms (3-8 A), significantly less than the separation observed in a conventional capacitor.
2. In a pseudo-capacitor, faradic electrochemical storage with electron charge transfer is carried out by oxygen-reduction, insertion, or electro sorption.

When the electrode is immersed in the electrolyte, opposite charges are generated instantaneously at the electrode-electrolyte interface, resulting in a charge separation between the electrode surface and the electrolyte in the form of double layers of electric charge. A charging layer with a specific polarity is formed on the electrode surface, while another charging layer with opposite polarity is formed in the electrolyte solution. These two charge layers are separated by a layer of solvent or water molecules, which acts as a dielectric, preventing the flow of charge between the electrode and the electrolyte (see Figure 2.3 in Appendix A. The double-layer capacitor starts the charging process when the power supply is connected to the electrodes (22).

2.1.3 Working principle and performance of supercapacitors

Generally, supercapacitors are ruled by the same basic principles as conventional electrostatic capacitors. The following equation represents the basic one for all capacitors:

$$\frac{\varepsilon_0 \varepsilon_r A}{d} \quad \ldots\ldots\ldots\ldots\ldots\ldots\ldots \text{ Eq. (2.1)}$$

Where ε_0 is the permittivity of free space, ε_r is the relative permittivity of the dielectric material, A is the surface area of the electrode, and *d* is the distance between the two electrodes see Fig. 2.4 in Appendix A. According to the relation in Eq. 2.1, the capacity of a capacitor can be controlled by adjusting (A), (ε_r), and (d) (28).

Similarly, supercapacitors are energy storage devices, but they differ from traditional capacitors in how they store charge. Supercapacitors do not store electric charge between two conductors separated by a dielectric material. Instead, it accumulates within the electric double layer formed at the interface between the electrolyte and the conductor. Once these supercapacitors are charged, the negative ions within the electrolyte will drift towards the positive electrode, whereas the positive ions will drift towards the negative electrode as shown in Fig 2.5 in Appendix A (18).

Generally, supercapacitors do not have dielectrics but use a thin coated layer on metal plates to keep positive and negative charges in place. The porous nature of the carbon layer coated this electrode gives the metal plates a larger surface area, allowing them to store additional charges. The carbon layer is much thinner than any dielectric used in a traditional capacitor, which means that the distance between the separate charges is much smaller in the supercapacitor. Combined, this minimal charge separation and increased plate surface area give the supercapacitor a much higher energy density than traditional capacitors (31).

The energy (E) of a capacitor can be calculated as:

$$E = \int \mathrm{CV}\, dV \quad \ldots\ldots\ldots\ldots\ldots\ldots\ldots \quad \text{Eq. (2.2)}$$

Where V is the applied voltage, also known as the potential window. For an ideal double-layer electric supercapacitor, C is not a function of V and Eq. (2.2) becomes:

$$E = \frac{1}{2}CV^2 \quad \ldots\ldots\ldots\ldots\ldots\ldots \quad \text{Eq. (2.3)}$$

Then the power (P) is calculated by:

$$P = \frac{E}{t_{dis}} \quad \ldots\ldots\ldots\ldots\ldots\ldots \quad \text{Eq. (2.4)}$$

Where (t_{dis}) is the time of discharging (29). Figure 1.1 shows a Ragone graphic diagram of the typical energy and power values of the supercapacitor compared to other energy storage systems such as fuel cells, batteries and capacitors (32).

Figure 1.1 shows that supercapacitors are positioned between traditional capacitors and batteries. Despite having a higher capacitance compared to standard capacitors, supercapacitors have not reached the energy densities seen in mid-to high-end batteries and fuel cells.

The rate at which charge is withdrawn (i) results in a corresponding decrease in voltage (V), so the rated power at a specific (i) value depends on the discharge state of the capacitor. The ratio of energy density to power density for a given capacitor depends on the load potential. A maximum power density relative to the energy density at a particular load state is defined by an open circuit potential which is also theoretically predicted for capacitors. For a given particular state of charge of a capacitor on discharge:

$$V = V_i - iR \quad \ldots\ldots\ldots\ldots\ldots\ldots \quad \text{Eq. (2.5)}$$

Therefore

$$P = iV = i(V_i - iR) \quad \ldots\ldots\ldots\ldots\ldots\ldots \quad \text{Eq. (2.6)}$$

and

$$E = \frac{1}{2}CV^2 = \frac{C}{2}(V_i - iR)^2 \quad \ldots\ldots\ldots\ldots\ldots\ldots \quad \text{Eq. (2.7)}$$

Based on these expressions, P and E can be optimized by maximizing V and C and minimizing R (33).

2.2 Carbon material as electrodes for supercapacitors

Capacity maximization is one of the major research areas to improve supercapacitor power output. Utilizing high-capacity materials plays a crucial role in achieving a high energy density. Simultaneously, ensuring both the electrode materials and the electrolyte solution exhibit high electrical conductivity is essential for optimizing flow efficiency (34). Carbon materials are widely considered attractive for their implementation as electrodes in supercapacitors due to its abundance, low cost, non-toxicity, chemical and thermal stability, high conductivity, and high specific surface area per unit mass. The effectiveness of these carbon materials depends on their structure, texture and shape (18). Carbon materials can be optimized by increasing the specific surface area, which can be done by Activation, Nano-structuring of nanotubes, optimization of porosity to match the sizes of electrolyte ions or Nano-structuring of Redox-active materials on interface surfaces. Further improvements can be achieved by pre-treating carbon to remove most surface functional groups or moisture affecting electrochemistry (33).

Figure 2.6 in Appendix A illustrates the forms of eight carbon allotropes. Fullerenes are a family of carbon allotropes consisting entirely of carbon atoms arranged in a concave sphere, ellipsoid, or tube-like structure. When these structures take on a cylindrical shape, they are known as buckytubes or carbon nanotubes. Fullerenes share structural similarities with graphite, characterized by interconnected hexagonal rings, but they also incorporate pentagonal or occasionally heptagonal rings, which prevent the sheet from being flat (35).

2.2.1 Activated Carbon

A carbon is activated by thermal or chemical processes to expand its adsorption capability. Activated carbon or activated charcoal is an absorbent element that entraps compounds in a gas or liquid states. It is the most commonly used purifying agent due to its remarkable efficiency. Activated carbon is used for many purposes as water purification, deodorization and air purification, treatment of people suffering from acute intoxication, etc. (36).

Activated carbon is commonly used as an electrode material in supercapacitors due to its low cost and extensive surface area. However, within activated carbon, many carbon atoms are not accessible to electrolytic ions, which makes them ineffective in terms of

their electrochemical capabilities. This key factor limits the specific capacitance that can be achieved with activated carbon electrodes. In addition, the limited electrical conductivity of activated carbon restricts its suitability for high power density supercapacitors and results in a lower specific capacitance per unit area (37). The combination of these two factors results in substantial internal resistance, which consequently leads to reduced power density in capacitors. Hence, there is a requirement for novel materials to address the drawbacks associated with activated carbon electrodes and improving the performance of supercapacitors. Carbon nanomaterials, with a particular emphasis on graphene and carbon nanotubes (CNTs), offer significant potential as alternatives to activated carbon for serving as electrode materials in high-performance supercapacitors (3).

2.2.2 Carbon Nanofibers

Carbon nanofibers, which have diameters between 3 to 100 nm and lengths between 0.1 and 1000 µm have a well-established history of causing disruptions during the catalytic transformation of gases containing carbon. The latest attention to these materials originates from their chemical similarity to carbon fullerenes and nanotubes and their potential unique applications (38). Carbon nanofibers possess tremendous application potential across various industries, including chemistry, materials science, composite reinforcement, and energy storage, because of their remarkable attributes, as a high surface-to-volume ratio, nanometer-scale diameter, and impressive mechanical characteristics (39). Carbon nanofibers can be generated by exposing carbon raw materials to elevated temperatures in the presence of Nano-sized metal particles. This process closely resembles the growth mechanism of carbon nanotubes. Nevertheless, carbon nanofibers exhibit a distinct geometry compared to concentric carbon nanotubes, as they possess an open core. Carbon nanofibers seem to be regularly piled in trimmed cone-shaped or flat layers along the fiber length (18). Synthesis pathways of CNFs are primarily chemical vapor deposition (CVD), templating, electro-spinning, phase separation and drawing. CNFs, which are prepared by diverse synthesis techniques, have various carbon forms and morphologies (39) see Fig. 2.7 in Appendix A.

Catalytic Chemical Vapor Deposition (CVD) is a commonly used method for yield carbon nanofibers through vapor-phase growth. Originally developed in the 1970s for diverse material production, it has undergone recent advancements specifically tailored

for producing carbon nanofibers (CNFs) (39). CNFs, which are yielded by CVD techniques or derived from polymeric fibers like rayon or polyacrylonitrile, can serve as effective conductive materials without requiring a binder. These electrodes demonstrate impressive electrical conductivities ranging from 200 to 1000 $(\Omega.cm)^{-1}$ and possess a high surface area (reaching 1000 – 2000 m^2/g once activated). However, their widespread use in commercial applications remains limited due to their elevated production costs (18).

2.3 Electrolytes for supercapacitors

The electrolyte emerges as an essential component of supercapacitors, playing a fundamental role in transferring and balancing charges between the positive and negative electrodes. The morphology and capacity values are significantly depend on the nature and concentration of electrolytes (20). The physical and chemical characteristics of electrolytes play a crucial role in the performance of electrochemical energy storage devices, affecting aspects such as capacity, performance, power density, safety and cyclability (41).

The interact between electrodes and electrolytes in all electrochemical processes considerably impacts the state of the electrode-electrolyte interface and the internal structure of active materials. Therefore, the properties of the electrolyte-solution system are essential for defining the electrochemical behavior of the supercapacitor device (21). Fig. 1.4 in Appendix A displays the electrolytes generally utilized in supercapacitors.

The capacity of electric charge storage relies on how easily ions can access the porous surface, making it crucial to find the right balance between ion size and pore size. Achieving an ideal pore size distribution on the electrode depends on matching the size of the ions in the electrolyte, emphasizing the need for precise selection of both electrodes and electrolyte components (18).

Until now, an ideal electrolyte that satisfies all the conditions of electrochemical devices has remained elusive. For example, supercapacitors employing aqueous electrolytes exhibit strong attributes like high conductivity and capacity but are hindered by low energy density, cycling stability issues, and concerns about leakage. On the other hand, organic electrolytes and ionic liquids, while capable of operating at high voltages, often suffer from significantly reduced ionic conductivity. Solid-state electrolytes offer a

solution to the potential leakage associated with liquid electrolytes but still encounter challenges related to their lower ionic conductivity (41).

2.3.1 Aqueous Electrolytes

Aqueous electrolytes showed a significant impact on capacity. Typically, aqueous electrolytes are classified into basic, neutral, and acidic electrolytes. Supercapacitors demonstrate more efficiency in acidic medium compared with neutral and basic electrolytes. The improved performance is due to the better ionic conductivity of the acid electrolyte (42). Aqueous electrolytes excel with regard to high ionic conductivity and capacity; however, they are constrained by their limited decomposition voltage, which restricts their working potential (43).

Aqueous electrolytes have smaller potential windows than non-aqueous electrolytes; approximately (1.0 - 1.3 V) while organic electrolyte and ionic liquid generally have (2.5 - 2.7 V) and (3.5 - 4.0 V) potential windows, respectively (44). Aqueous electrolytes typically exhibit high conductivity in comparison to non-aqueous and solid electrolytes. This high conductivity can be primarily attributed to several factors, including the low dynamic viscosity of aqueous electrolytes. It is mainly related to ionic mobility, charge carrier concentration, the elemental charge, and the magnitude of the charge valence of mobile ions. These variables are intricately linked to factors such as solvation effects, the movement of solvated ions, and the lattice energy of the salt (41).

2.3.2 Characteristics of the Dead Sea water

The Dead Sea is a rare geological and natural phenomenon located on the longest continental rift line in the world. It is a closed sea that does not connect to the surrounding outer seas of the region, located on the border between Palestine and Jordan (45). The Dead Sea is an enclosed hyper-saline lake located in the deepest part of the Jordanian valley. It is about 80 km long, and 18 km wide, with a surface area of about 1,020 km^2 and its water surface level is about 400 m below sea level, making it the lowest surface level on the earth (46).

Dead Sea water is characterized by a high salinity of up to 340 g/liter, which represents a very important value because the salinity there is ten times greater than the salinity of the

seas and oceans. The Dead Sea stores an enormous wealth of a large group of salts and minerals of great economic value for many modern industries (45).

The pH of the Dead Sea is approximately 6, and it contains an unusually high mineral salt concentration of about 348 grams per liter. Compared to other oceans and seas, the Dead Sea contains high levels of certain elements, notably Chloride (at 212.4 g/l), Magnesium (at 40.65 g/l), Sodium (at 39.15 g/l), Calcium (at 16.86 g/l), Potassium (at 7.26 g/l), and Bromide (at 5.12 g/l). In contrast, it has notably lower concentrations of Sulphate (at 0.47 g/l) and Bicarbonate (at 0.22 g/l) (47).

Total dissolved solids (TDS) are the sum of organic and inorganic substances, such as metals, minerals, salts and ions, that have been dissolved in water, and indicate the salinity of the seawater that was collected (50). Salinity, temperature and frequency are parameters on which the conductivity of seawater depends (48, 49). For the collected Dead Sea water, the calculated value of TDS was 60.1 g/L. When comparing the measured data of the Dead Sea water and distilled water, a significant difference in their conductivity was observed. The conductivity of the Dead Sea water is 3 to 4 times higher than that of distilled water. Specifically, the conductivity is 4.608 $(\Omega.\ m)^{-1}$ for Dead Sea water and 0.0067 $(\Omega.\ m)^{-1}$ for distilled water, which is expected due to the high salinity of the Dead Sea water (51).

2.4 Electrochemical characterization

Nanomaterials are very promising for use in high-energy storage devices due to their exceptional qualities, so they have recently aroused the scientific interest. Various characterization techniques have been developed to assess the proper functioning of nanomaterials in the applications for which they are intended. Electrochemical analysis is the most efficient method for evaluating the efficiency of these materials in energy storage applications and understanding mechanisms associated with processes such as charge transfer, mass transfer, electrolyte transport, electron transport, and more (52).

All electrochemical characterization is carried out with the assistance of electrochemical methods, CV, GCD, EIS and other similar techniques.

2.4.1 Cyclic voltammetry (CV)

Cyclic voltammetry (CV) serves as a fundamental electrochemical assessment for materials. In this technique, the current is monitored while sweeping the voltage potential back and forth within predefined limits, encompassing both positive and negative directions. The information obtained from the CV can offer valuable data about the electrochemical properties of the material. The cyclic voltammogram displays distinctive redox peaks, as seen in Figure 2.8 in Appendix A, which can be used to anticipate the capacitive properties of the electrode. This enables the identification of the potential at which the material undergoes oxidation and reduction processes (52).

CV has emerged as a crucial technique for evaluating the performance of supercapacitors due to its suitability for determining cycle life. The CV provides a comprehensive insight into how capacitance behaves when measured at various sweep rates while also offering valuable information regarding the material's specific capacitance. When using CV, the voltage is swept between two values at a constant rate (s = dV/dt) and the resultant current (I) is measured as a function of time. Using equation (2.1), the capacitance can be calculated. To learn more about internal resistance effects and the ensuing dissipative losses, one can study the voltammogram as a function of S.

$$C_s = \frac{1}{SmΔV} \int IdV \ldots\ldots\ldots\ldots\ldots\ldots . \quad Eq.(2.8)$$

Where (I) represents the average current and (ΔV) the voltage window, (S) is the scan rate in (mV/s), (m) for the electrode's total mass of active material (18) and $\int IdV$ is the area under the I-V curve (51).

2.4.2 Galvanostatic Charging Discharging (GCD)

Supercapacitors have also been characterized by Galvanostatic charging/discharging, as they are physically linked to capacitive charging. In the case of an ideal capacitor, it is feasible to anticipate a triangular response at constant current, with a slight deviation at the apex caused by the resistance of the solution. The empirical results, however, significantly differ from the theoretical model, raising questions about the accuracy of the simple capacitor model in interpreting the data. Procedures were the same as those used with the CV in order to analyze the GCD, except that current was employed in place of voltage as a stimulus for an electrochemical cell (53). With this technique, a constant

charging current is applied until a maximum potential is obtained, and then a discharge current of equal magnitude is applied until a minimum potential is reached. The potential is tracked as a function of time. GCD tests may more closely reflect actual system performance since a constant current is employed instead of a constant voltage sweep rate as in CV. Figure 2.9 in Appendix A displays a few common Galvanostatic charge/discharge plots. The charge/discharge plot for an ideal supercapacitor should be symmetrical and has a constant slope Fig. 2.9a in Appendix A (54).

The following equations are used to compute the specific capacitance (C_s), power density (P_d), and energy density (E_d) based on the Galvanostatic charge/discharge curve:

$$C_s = \frac{I\Delta t}{m\Delta V} \quad \ldots\ldots\ldots\ldots\ldots\ldots\ldots\ldots. \quad Eq.(2.9)$$

$$E_d = \frac{1}{2} \times C_s \times (\Delta V)^2 \quad \ldots\ldots\ldots\ldots\ldots\ldots\ldots. \quad Eq.(2.10)$$

$$P_d = \frac{E_d}{\Delta t} \quad \ldots\ldots\ldots\ldots\ldots\ldots\ldots\ldots. \quad Eq.(2.11)$$

Where C_s (F/g) represents specific capacitance, E_d (Wh/kg) represents energy density, P_d (W/kg) represents power density, I (A) is discharge current, Δt (s) is discharge time, ΔV is the potential window and m (g) is the active mass (the total mass of the two electrodes) (26, 55).

Due to the equivalent series resistance (ESR) of the EDLC, the voltage drop (V_{drop}) that is seen in figure 2.9(c) is caused when the current is switched from charging current (+I) to discharging current (-I). So using Ohm's law, ESR can be calculated from V_{drop} as follows (19):

$$ESR = \frac{V_{drop}}{2I} \quad \ldots\ldots\ldots\ldots\ldots\ldots\ldots\ldots \quad Eq.(2.12)$$

2.4.3 Electrochemical Impedance Spectroscopy (EIS)

EIS is a powerful method used to analyze electrochemical systems, including corroded surfaces, fuel cells, solar cells, batteries, sensors, and biological systems (56). According to this technique, the behavior of an electrode when exposed to a particular electrolyte can be explained by considering its electrical characteristics, including resistance and capacitance. By analyzing these parameters, we can assess how the electrode behaves in relation to a specific chemical reaction and its capacity to sustain electron transfer based on its impedance values (57).

A low amplitude alternating current (AC) signal is employed in EIS to examine the impedance characteristics of a cell. This AC signal is varied over an extensive frequency range in order to generate an impedance spectrum describing the response of the electrochemical cell (58).

A numerical reproduction of the Nyquist plot is achieved by employing a physicochemical transport model. This model takes into account three fundamental elements: firstly, it addresses the generation of the EDL at the interface between the electrode and the electrolyte. Secondly, it examines the flow of electric charge within the electrode. Lastly, it investigates electro-diffusion processes within both binary and symmetric electrolyte systems. The Nyquist plot can be used as a valuable tool for determining key parameters such as electrolyte resistance, electrode resistance, and equilibrium differential capacitance (59).

The semi-circular behavior developed at high frequencies can be a result of either the charge-transfer mechanism and/or fluctuations in contact resistances and double-layer capacitance. The lower frequency range exhibits a linear pattern, representing diffusive processes, with an ideal supercapacitor having a 90° angle. Connecting these two regions is a mid-frequency line at a 45° angle, corresponding to the porous characteristics of the electrode when it's fully saturated with the electrolyte (18).

The R_A resistance in Figure 2.10 in Appendix A is internal resistance that is generated due to the presence of equivalent series resistance (ESR), which encompasses the electrode resistance, the resistance within the bulk electrolyte, and the resistance occurring at the interface between the electrode and the current collector. The charge

transfer resistance has been assigned as the diameter of the semi-circle $R_{AB} = R_B - R_A$ which involves the combined effects of the electrolyte resistance within the porous electrode structure, the resistance within the electrode itself, and the resistance at the interface where the electrode contacts the current collector. Also, the resistance $R_{BC}$is referred to as "equivalent distribution resistance" (59). The radius of the semicircle ($= R_{AB}/2$) indicates the polarization resistance (R_P) and provides information on the accessibility of the electrolyte in the pores. R_B represents the charge or electrolyte transfer resistance, and R_C is the contact resistance between the thin electrode and the current collector (18). The presence of a vertical line at low frequencies around point C can be attributed to the dominant capacitive behavior of the EDL that develops at the interface between the electrode and the electrolyte. This point where the vertical line intersects with the X-axis, representing R_C, is often referred to as the total resistance of the electrode or device (59).

EIS is measured using a small-amplitude AC signal over a wide frequency range. The applied potential as a function of time V_t, with amplitude V_o and radial frequency ($\omega = 2\pi f$), varies over time as follows:

$$V_t = V_\circ \sin(\omega t) = V_\circ \, Im(e^{j\omega t}) \quad \dots\dots\dots\dots\dots\dots\dots\dots \quad Eq.(2.13)$$

Because the equivalent supercapacitor circuit has both a resistor and a capacitor, the input current signal will have a phase shift (ϕ), as below (19):

$$I_t = I_\circ \sin(\omega t + \varphi) = I_\circ \, Im(e^{j(\omega t - \varphi)}) \quad \dots\dots\dots\dots\dots\dots\dots\dots \quad Eq.(2.14)$$

Where I_o is the current signal's amplitude.

The overall impedance Z of the supercapacitor can be computed as:

$$Z = \frac{V_t}{I_t} = \frac{V_\circ \, Im(e^{j\omega t})}{I_\circ \, Im(e^{j(\omega t - \varphi)})} = Z_\circ(cos\varphi + jsin\varphi) = Z_{re} + jZ_{im} \quad \dots\dots\dots \; Eq.(2.15)$$

Where Z_{re} and Z_{im} (measured in $\Omega.m^2$) are the real and imaginary components of the complex impedance (59).

The following equation can be used to calculate the specific capacitance (C_s) of one electrode (13):

$$C_s = 4\left(\frac{-1}{2\pi f Z_{im} m}\right) \quad \ldots\ldots\ldots\ldots\ldots\ldots\ldots \qquad \text{Eq. (2.16)}$$

The following equation can be applied to calculate the relaxation time that points to the transition of an electrochemical capacitor from purely resistive to purely capacitive state (18, 19, 60):

$$\tau_\circ = \frac{1}{f_0} \quad \ldots\ldots\ldots\ldots\ldots\ldots\ldots \qquad \text{Eq. (2.17)}$$

Where f_0 is the knee frequency at phase shift 45° (18).

The time constant (τ) demonstrates the charging response of the supercapacitor and is calculated by the following equation (20):

$$\tau = RC = (ESR)C \quad \ldots\ldots\ldots\ldots\ldots\ldots\ldots \qquad Eq.(2.18)$$

2.5 Porosity and surface Area of Materials

"Activated carbon" refers to a category of substances distinguished by their substantial internal surface area and porosity, which imparts them with a remarkable ability to absorb chemicals from both gases and liquids. This increased porosity and expansive surface area are achieved through the process of activation, which can be conducted physically or chemically. Adsorption isotherms are utilized to evaluate pore volume and surface area in different porosity systems, evaluations of the adsorbent's surface chemistry, and basic information about the effectiveness of industrial carbon used in separation and purification processes (61).

The determination of the performance of a supercapacitor is significantly influenced by the electrode surface and the total resistance of the cell. Therefore, the morphology of the electrode emerges as a crucial factor in this process, along with the nature of the electrolyte (7). It has been demonstrated that capacitance is related to the morphology, porosity, and surface chemical characteristics of porous carbons used as electrode materials (62).

The pore size standard established by IUPAC is divided into three main categories: macropores (>50 nm), mesopores (2-50 nm) and micropores (<2 nm) (9). In order to have a large specific surface area, materials with high porosity are recommended. In addition, the pore size distribution (PSD) of the electrode must correspond to the size of the ions forming the electrolyte to increase the number of ions that enter the pores (7).

Analytical methods, such as the Brunauer-Emmett-Teller (BET) and Barrett-Joyner-Halenda (BJH) theories, can be used to determine the pore characteristics of a material, such as size, volume and surface area. The BET analysis allows to calculate the total specific surface area in square meters per gram (m^2/g), examining both the pore area and the external surface by nitrogen adsorption isotherms. Instead, BJH analysis is employed to determine the specific pore area and volume, providing information on the pore size distribution through nitrogen adsorption and desorption techniques (18).

The adsorption isotherms typically follow one of the six categories depicted in Fig. 2.11 in Appendix A. Type I isotherm results when a monolayer of adsorbate molecules is adsorbed on a nonporous substance or when a micropore filling process dominates the adsorption. The Langmuir-type isotherm is another name for this kind of isotherm. Nonporous or macroporous adsorbents exhibit Type II, an S-shaped isotherm. This isotherm has an inflection point that marks the end of the monolayer formation and the start of the multilayer formation. The Type III adsorption isotherm, which is typical of nonporous or macroporous adsorbents, indicates weak adsorbent-adsorbate interactions. A mesoporous adsorbent typically exhibits the Type IV isotherm, which is comparable to the Type II isotherm. It differs from the other varieties in that it has a hysteresis loop linked to capillary condensation. An adsorbent that is nonporous or macroporous typically exhibits the Type V isotherm. Similar to the Type III isotherm, Type V isotherm is seen when the adsorbent-adsorbate interaction is weak. The last isotherm displayed is a stepped Type VI isotherm. This type is rarely observed and indicates non-porous samples with a completely uniform surface (18, 63).

The total area that is provided by all open pores is known as the "specific surface area" (SSA) of a solid porous material. The BET analysis, which is based on the amount of N_2 gas molecule adsorption and desorption, is used to calculate the specific surface area (18, 19).

The physical adsorption of a gas onto the surface of a solid sample and the measurement of the amount of adsorbate gas corresponding to a monolayer on the surface are used to determine a sample's specific surface area. Adsorption measurements are typically performed at low temperatures because the amount of gas adsorbed at a given pressure tends to rise as temperature decreases. The liquid nitrogen boiling point of 77 K is used for measurement. The BET adsorption isotherm equation is applied to the data as follows (64-66):

$$\frac{1}{\left[V_a\left(\frac{P_0}{P}-1\right)\right]} = \frac{C-1}{V_m C} \times \frac{P}{P_0} + \frac{1}{V_m C} \quad \ldots\ldots\ldots\ldots\ldots \quad \text{Eq. (2.19)}$$

Where P, in mm of mercury, stands for the partial vapor pressure of the adsorbate gas in equilibrium with the surface at 77 K, and P_0, in mm of mercury, stands for the saturation pressure of the adsorbate gas, V_a is the volume of gas adsorbed at standard temperature and pressure (STP, 273.15 K, and 760 mm of mercury); V_m is the volume of gas adsorbed at STP that forms a monolayer of surface coverage; and C is a dimensionless constant that is related to the enthalpy of adsorption of the adsorbed, also expressed in milliliters (mL). A value of V_a is determined at least at each of three different P/P_0 values (64, 66).

Plotting $\left(\frac{1}{\left[V_a\left(\frac{P_0}{P}-1\right)\right]}\right)$ vs. (P/P_0), as in Fig. 2.12 in Appendix A, will result in a straight line that is typically between $0.05 \leq P/P_o \leq 0.35$ (19, 65).

In a BET plot, the slope (s) and y-intercept (i) are (19, 64, 65):

$$s = \frac{C-1}{V_m C} \quad \ldots\ldots\ldots\ldots\ldots\ldots\ldots \quad Eq.(2.20)$$

$$i = \frac{1}{V_m C} \quad \ldots\ldots\ldots\ldots\ldots\ldots\ldots \quad Eq.(2.21)$$

The volume of absorbed N_2 monolayer (V_m) can be estimated using *(s)* and *(i)* as follows:

$$V_m = \frac{1}{s+i} \quad \ldots\ldots\ldots\ldots\ldots\ldots\ldots \quad Eq.(2.22)$$

After which the total surface area (S_t) can be calculated using:

$$S_t = \frac{V_m N\, A_{cs}}{V} \quad \ldots\ldots\ldots\ldots\ldots\ldots\ldots\ldots \quad Eq.(2.23)$$

Where V is the molar volume of a gas at STP (22411 cm^3/mole), N is the Avogadro's number (6.023×10^{23}), and A_{CS} is the cross-sectional area of the N_2 molecule (0.162 nm^2).

The specific surface area (SSA) (m^2/g) can thus be determined by:

$$SSA = \frac{S_t}{m} \quad \ldots\ldots\ldots\ldots\ldots\ldots\ldots\ldots \quad Eq.(2.24)$$

where *m* represents the entire mass of the porous material.

2.6 Previous Studies

Many studies have addressed the subject of supercapacitors from different aspects. Here, the researcher reviews some of the studies that were used to prepare the theoretical framework for this study, including:

In the study conducted by Daraghmeh et al. (2017), a comparison was made between carbon nanofibers (CNFs) and activated carbon (AC) as materials for symmetrical supercapacitors in an aqueous electrolyte. Symmetrical supercapacitors were manufactured using similar proportions of 7% by weight of PVDF polymeric binder in an aqueous electrolyte. The electrodes prepared with CNFs and AC exhibited Brunauer Emmett Teller (BET) surfaces of 83 m^2/g and 1042 m^2/g, respectively. The dominant porous structure for CNFs was mesoporous, while for AC it was microporous. In aqueous solution, AC provided a specific capacitance of 334 F/g, while CNFs showed a capacitance of 52 F/g at a scan rate of 5 mV/s. The results pointed out that the higher conductivity of CNFs compared to AC resulted in a higher retention of specific capacitance, especially at fast scan rates up to 500 mV/s. The measured ESR was significantly lower for CNFs (0.28 Ω) compared to AC (3.72 Ω). In addition, it was observed that CNFs offered a higher specific power (1860 W/kg), while AC provided a higher specific energy (18.1 Wh/kg). The CNFs and AC supercapacitors demonstrated excellent discharge and charge stability over 2500 cycles (13).

Holla & Selvakumar (2018) investigated the impact of various electrolytes on the performance of supercapacitors made from electrode materials with single and multiple layers based on multi-walled carbon nanotubes/polyaniline composites. They conducted electro-polymerization followed by the fabrication of symmetric supercapacitors based on single-layer and multi-layer carbon nanotubes/polyaniline (MWCNT/PA). The morphology and capacitance values are highly dependent on the nature and concentration of electrolytes. The presence of micro and mesopores in MWCNT provides space for the deposition of polyaniline. Extended conjugation results from the overlap of π- electron cloud with the hybrid sp2 carbon network of MWCNT, featuring three-layered quinoid-doped PA cycles with three dopants, which leads to the highest capacitance of 333 F/g and good charge-discharge cycle behavior with an 85% retention of charge over 1000 cycles for the symmetric supercapacitor based on the multi-layer composite material (20).

Pal et al. (2019) conducted a comprehensive discussion of electrode-electrolyte interactions in supercapacitors and hybrid battery-supercapacitor systems. The research explored several factors that have a significant impact on the overall performance of these devices, including ionic mobility, ionic conductivity, diffusion coefficients, ionic solvation, the radius of hydrated and naked ions, viscosity, dielectric constant, electrochemical and thermal stability, and dispersion interactions. The article underscored the essential criteria for formulating improved electrolytes and shed light on the persisting challenges that must be addressed to develop advanced supercapacitor technology (41).

Iqbal, Zakar, and Haider (2020) conducted a detailed examination of how aqueous electrolytes impact the energy storage capabilities of electrochemical supercapacitors. The findings showed that supercapacitor electrode materials exhibit exceptional performance when immersed in aqueous acidic electrolytes, thanks to their exceptional ionic conductivity. While supercapacitor electrodes with neutral aqueous electrolytes exhibit lower capacity due to a decrease in their molar ionic conductivity, this emphasizes the vital role of electrolyte selection as a critical factor in achieve high-efficiency energy storage devices, which are essential for future technical advance (42).

Shahrouj's (2021) research investigated the utilization of active carbon/graphene nanoplates as electrodes for supercapacitors with varying aqueous electrolytes, namely H_2SO_4, Na_2SO_4, and KOH. The study aimed to assess how altering the electrolyte affected

the supercapacitor's capacitance when utilizing these active carbon/graphene nanoplate electrodes. To do this, electrode pellets composed of active carbon and graphene nanoplates were prepared and subjected to analysis in conjunction with the three different electrolytes. Shahrouj employed a universal Potentiostat or Galvanostat to conduct CV, GCD, and EIS tests on the supercapacitor. The findings demonstrated that the highest recorded capacitance, 320.3 F/g, was obtained when using an H_2SO_4 electrolyte solution and measuring it through CV at a scan rate of 5 mV/s. Additionally, this electrode exhibited the lowest ESR, measuring at 0.311 Ω, as determined by the EIS method. As a result, the electrode tested with the H_2SO_4 electrolyte displayed the highest specific energy and specific power, registering at 14.82 Wh/kg and 4177.8 W/kg, respectively (19).

Ishtaiwi, Hajjyahya, and Habbash (2021) utilized dielectric measurements to gather information on the conductivity, permittivity, and loss tangent of water extracted from the Dead Sea. These specific dielectric properties were assessed through the use of a Vector Network Analyzer (VNA) and the Four Probe method, all at a standard room temperature of (25°C). The data collected was examined across a frequency range spanning from (200 MHz to 9 GHz) and was subsequently compared to data acquired from distilled water. The findings illuminated substantial disparities in dielectric characteristics between the two water samples. It was observed that the conductivity of Dead Sea water significantly surpassed that of distilled water, a result in line with expectations given the high salinity of Dead Sea water (51).

Chapter Three
Experimental Work

A supercapacitor electrode using a composite of activated charcoal (AC) and carbon nanofibers (CNFs) was prepared. The impact of aqueous electrolytes (1 M H_2SO_4, 6 M KOH, and Dead Sea water) on electrode capacity has been studied to optimize the electrolyte solution that gives the best specific capacitance, energy density, power density, and cycling stability. To achieve this, a range of electrochemical techniques were employed, utilizing a universal Potentiostat/Galvanostat. Furthermore, the study examined the surface and internal morphological and structural characteristics through scanning electron microscopy (SEM) and investigated the porosity of the electrode material by analyzing the adsorption and desorption of N_2 gas. To perform this study, several materials and equipment were used. An explanation of these materials and devices is given below.

3.1 Chemicals and Materials

All solvents and chemicals were utilized in their analytical grade without requiring any further purification. Distilled water was used to prepare stock solution of 6 M KOH and 1 M H_2SO_4. Table 3.1 presents the Chemicals and materials used in this study.

Table 3.1

Chemicals and materials used in the study

Chemicals & Materials	Purity	The source
Distilled water		
KOH (pellets)		Merck Millipore
H_2SO_4	98%	Merck Millipore
Acetone	≥99.7%	Sigma Aldrich
Activated Carbon (AC)		Donau Carbon
Carbon Nanofibers (CNFs)	>98% carbon basis	Sigma Aldrich
Poly(vinylidene difluoride) (PVDF)		Sigma Aldrich

3.2 Equipments, Devices and Instruments

The needed equipment, devices, and instruments that were available at An-Najah National University that were used in preparing the supercapacitor electrodes and electrolytes and studying the electrochemical characteristics of the electrodes in various electrolyte solutions are: glassware, electronic scale, glass fiber separator-M 5V5 (from Alter-Lab), Potentiostat (PGZ402), Swagelok cell, magnetic stirrer, agate mortar, ultrasonic cleaning device (Elmasonic S10H), dry oven (Ari J. Levy), and hydraulic press (Shimadzu).

Some of the experimental work was done at Barcelona University laboratories, which was related to the inner morphology, surface morphology, structure and porosity of the electrodes. The following devices have been used at Barcelona University laboratories:

1. Scanning Electronic Microscope (SEM, Jeol J-7100).
2. Brunauer-Emmett-Teller analyzer (BET, TriStar 3000 V6.04A).

3.3 Preparation of electrode pallets

The AC/ CNFs composite electrode pellets to be used in two-terminal Swagelok supercapacitor cells were prepared through the following steps:

1. Using an agate mortar, AC (90 wt.%) and CNFs (10 wt.%) were milled.
2. A mixture was prepared from AC and CNFs by using a 5% concentration of PVDF as a binder.
3. A mixture of AC/CNFs containing 15 ml of acetone was prepared in a beaker and stirred using a magnetic stirrer to create a slurry.
4. The slurry was subjected to ultrasonic agitation in an ultrasonic bath for a duration of 20 minutes at a temperature of 35°C.
5. The slurry was dried in an oven set at 70°C for 1 hour.
6. Once dried, the slurry was further processed by milling it using an agate mortar, resulting in the formation of a powder.
7. This powder was subsequently utilized to create circular electrode disks using a mold, and hydraulic pressure was applied at 8 tons during the molding process.

8. The mass of each electrode was determined using an electronic balance, with calculated masses falling within the range of 0.025 to 0.03 grams and each electrode having a diameter of 10 mm.

3.4 Preparation of electrolytes

Four types of electrolytes were prepared and used to examine the different electrochemical properties of the supercapacitor. These electrolytes are:

1. 1 M H_2SO_4 solution (by adding distilled water, 5.44 ml of 98% sulfuric acid was diluted to 100 ml to prepare a 1 M H_2SO_4 solution).
2. 6 M KOH solution (by dissolving 33.66 g in 100 ml of distilled water to prepare a 6 M KOH solution).
3. Dead Sea water
4. Concentrated Dead Sea water, made by heating 100 ml of Dead Sea water until it was reduced to 50 ml.

3.5 Electrochemical characterization

The assessment of the electrochemical properties of the composite electrode (AC/CNF) has been carried out by various test techniques, such as CV, GCD and EIS. The four different electrolyte solutions were initially prepared within the Swagelok as follows:

1. A glass fiber separator disk was carefully cut.
2. The glass fiber separator was submerged in the chosen electrolyte for 2 minutes.
3. The soaked glass fiber was positioned between the electrodes.
4. The Swagelok cell was closed tightly to avoid any spaces between electrodes and fix all parts well.
5. Following the assembly of the Swagelok cell, it was connected and subjected to testing using the Potentiostat.

In this work, the electrochemical characterization (CV, GCD, and EIS) of the electrode was performed in a Swagelok cell with a glass fiber separator-M 5V5 using a PGZ402 Potentiostat. The Potentiostat was connected to the Swagelok cell using two terminal mode. The Swagelok cell's anode was linked to the work and sense leads of the

Potentiostat, and the cell's cathode was connected to the auxiliary and reference leads. The data was collected using Potentiostat VoltaMaster 4 program. Below is a brief description of the electrochemical experiments carried out.

1. A potential that changes progressively from 0 to 1 V at various scan rates (5, 10, 20, 50, 100, and 150 mV/s) was used for cyclic voltammetry (CV). Four supercapacitor cells of various electrolyte solutions underwent 100 CV cycles.
2. Different current values were used with the Galvanostatic Charge Discharge (GCD) method (10, 20, 40, 50, 70, 100 and 150 mA). A range between 0 and 1 V was specified for the response voltage during charging and discharging.
3. The Electrochemical Impedance Spectroscopy (EIS) method was utilized to investigate the supercapacitor cell's impedance when an AC signal with various input frequencies was applied. A 20-mV amplitude AC sine wave with frequency ranges of 10 mHz to 100 kHz was used to every cell made up of various electrolytes.
4. For each supercapacitor cell made with a different electrolyte, the cyclic stability and reversibility were examined for 100 cycles using the CV technique and 1000 cycles using GCD.
5. Finally, the Origin Pro 2022b application was used to analyze the data gathered via all methods.

3.6 The Surface Morphology of AC/CNFs Composite Electrode Material

Scanning electron microscopy (SEM) is usually performed to study the crystalline structure of solids and examine their specific morphology. The excited electron beam of a SEM scans a sample in a raster sweep pattern to create an image of it. During each sweep, the atoms that make up the sample generate signals that provide details about its surface topography, composition, and other characteristics like electrical conductivity (18).

In this research, the surface morphology of the AC/CNFs composite electrode was investigated by SEM. The SEM image was created by scanning the electrode material with an excited electron beam. A slot was used to adjust the electron beam's size in order to properly target the sample's surface. Secondary electrons were emitted from the sample's surface as a result of the electron beam's interaction with its surface atoms. These

electrons were detected and studied to learn more about the electrode material's surface properties and electrical conductivity.

3.7 The Porosity of AC/CNFs Composite Electrode Material

The physical interactions of solids and the chemical reactivity of materials with liquids and gases are both significantly influenced by porosity. For porous electrodes made for supercapacitors, different methods of gas adsorption and desorption are employed to study the specific surface area (SSA), total pore volume, and pore size distribution (PSD). The SSA of the pores can be studied using the Brunauer-Emmett-Teller (BET) method (19).

The porosity of the AC/CNFs composite electrode was studied by the adsorption and desorption of N_2 gas at the boiling temperature of liquid nitrogen (77.3 K). N_2 is utilized since its molecular size is well known, so it is easy to determine the surface area and volume of pores. Additionally, because nitrogen is an inert gas, it doesn't react with the material's surface while being measured. A BET analyzer (TriStar 3000 V6. 04A) was used to measure the porosity. The amount of absorbed N_2 gas was measured as a function of the relative applied pressure (P/P_0) at STP (273.15 K and 1 atm.). The material's pores can be almost entirely filled with condensed liquid N_2 since the relative pressure can range from 0 to ~ 0.999. The data was evaluated using the BET method to calculate the total specific surface area (S_{BET}).

Chapter Four

Results and Discussion

Various experiments have been carried out on the AC/CNFs composite supercapacitor electrode to assess its diverse characteristics in different electrolyte solutions, namely 6 M KOH, 1 M H_2SO_4, and varying concentrations of Dead Sea Water. (CV), (GCD), and (EIS) were employed to determine the electrochemical properties, while a porosity analysis was implemented to assess the material's physical interaction.

4.1 Electrochemical Characterization

Using a two-electrode Swagelok cell and a PGZ-402 Potentiostat, the electrochemical characteristics of the AC/CNFs supercapacitor electrodes were investigated. The supercapacitor was tested with several electrolytes, including 6 M KOH, 1 M H_2SO_4, and different concentrations of Dead Sea water. To assess the supercapacitor's performance, the specific capacitance was measured using different techniques, including CV, GCD, and EIS, to enrich the research and raise the credibility of its results.

4.1.1 Cyclic Voltammetry (CV)

Cyclic voltammetry (CV) was performed using a potential that gradually changes from 0 to 1 V at several scan rates (5, 10, 20, 50, 100, and 150 mV/s). Four supercapacitor cells were subjected to 100 CV cycles in different electrolyte solutions. Each supercapacitor electrode, which was made up of 90% AC and 10% CNFs, was investigated using a glass fiber separator and a variety of electrolytes (6 M KOH, 1 M H_2SO_4, and various concentrations of Dead Sea water).

The electrodes' cyclic voltammetry response was assessed at various scan speeds ranging from 5 to 150 mV/s. The voltammogram shape for all of the cells in the sample is shown in Fig. 4.1(a-d), and It possesses a rectangular shape, displaying no deviations or peaks, which suggests that its supercapacitive properties are not influenced by redox reactions and are primarily driven by electrostatic mechanisms. Additionally, this shape signifies minimal internal resistance, aligning with the characteristic voltammogram of electric double-layer capacitance (18). Figure 4.1 (a-d) displays the results of the CV analysis for each electrolyte, along with a comparative assessment between them. Semi-rectangular CV curves are observed at low scan rates (5-20 mV/s). This denotes the type of electric

double-layer capacitor and, as a result, the supercapacitor's high capacitive characteristics, as well as its fast current response to potential change. At higher scan speeds (50-150 mV/s), a deformation from a rectangular form can be detected. This is explained as follows: as the scan rate increases, the current density increases due to an increase in ion mobility, and the ions accumulate at the pore surface into the diffusion layer, making it difficult for the ions to enter deeply into the vacant pores or even not enter the pores, particularly tiny pores. This leads to a decrease in the surface area exposed to ions, resulting in a lower specific capacitance for the supercapacitor electrode (14, 62).

Figure 4.1

Cyclic voltammetry curves for AC/CNFs supercapacitor

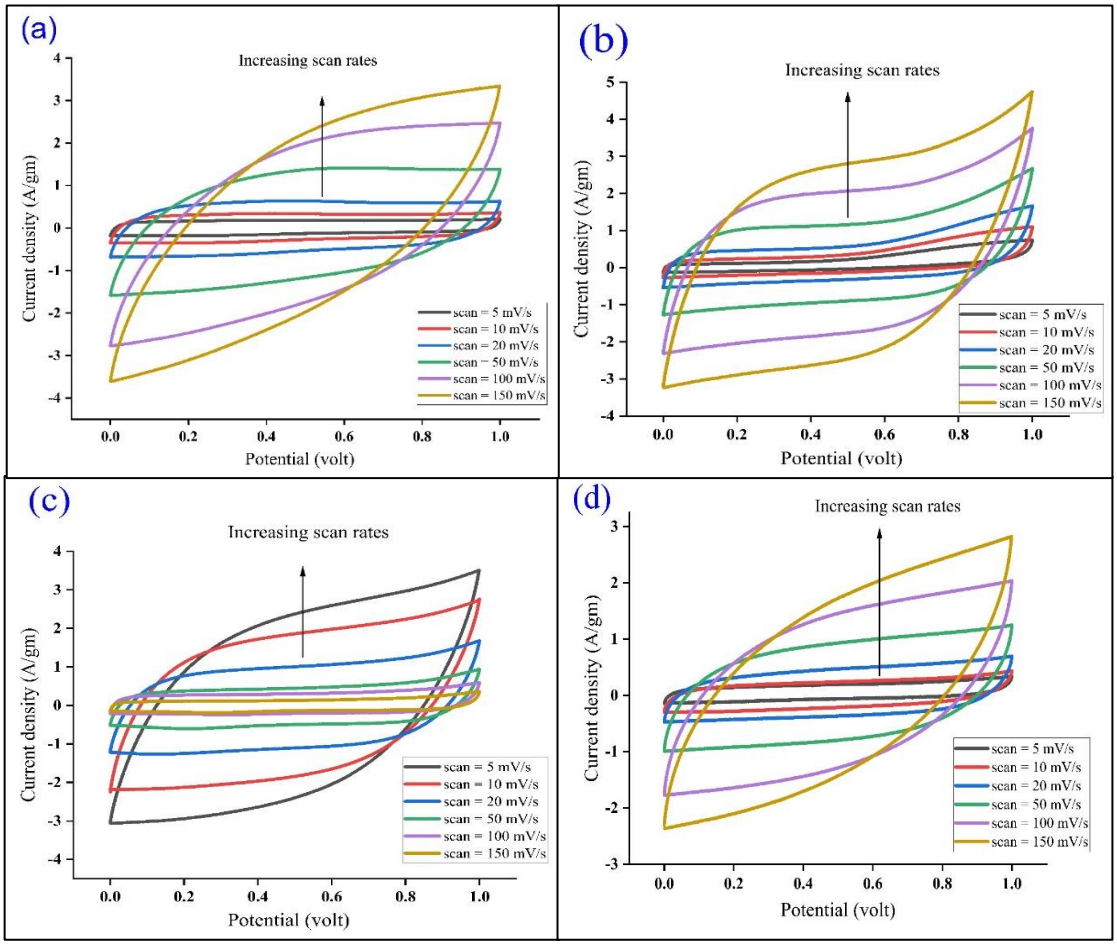

(a) 1 M H_2SO_4, (b) 6 M KOH, (c) Dead Sea Water, (d) Concentrated Dead Sea water electrolytes.

Fig. 4.2 depicts a comparison of four samples at a 100 mV/s scan rate. The area inside the CV curve for electrodes with 1 M H_2SO_4, 6 M KOH, and Dead Sea water electrolytes was similar, indicating higher stored charges and thus higher specific capacitance (Cs),

hile the area inside the CV curve for electrodes with concentrated Dead Sea water electrolytes was the lowest, indicating the lowest stored charges and thus the lowest Cs. The lowest Cs of the supercapacitor with concentrated Dead Sea water electrolytes is due to the fact that ion mobility reduces considerably as ion concentration increases.

Figure 4.2

Comparison of cyclic voltammetry curves for AC/CNFs supercapacitors using: 1 M H2SO4, 6 M KOH, Dead Sea Water, and concentrated Dead Sea Water electrolytes at scan rate = 100 mV/s

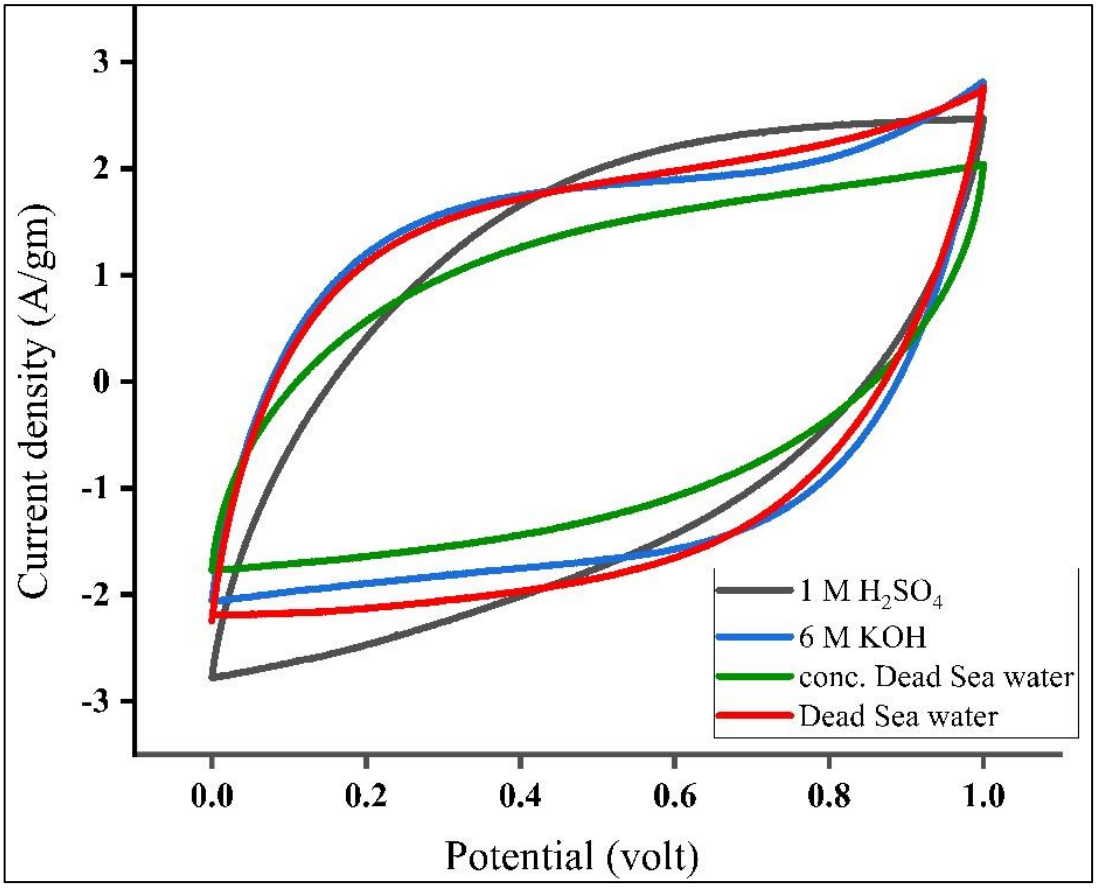

The specific capacitance was determined for each sample at different scan rates, as reported in Table 4.1 and shown in Fig. 4.3. Cs for electrodes with 6 M KOH was found to be slightly greater than that for other electrolytes at a (5 mV/s) scan rate, with a maximum specific capacitance of (157.86 F/g) at the same scan rate. This result contradicts the results of previous studies, including the study of Shahrouj (2021), which indicated that the Cs of the supercapacitor was higher with H_2SO_4 electrolyte than with KOH electrolyte at all scanning rates. Perhaps this difference is due to the difference in the type of electrode—Shahrouj used an AC/GNPs composite electrode, while this study

used an AC/CNFs composite electrode—or this may be due to an error in the experiment at the rate of 5 mV/s.

Table 4.1

The Cs of AC/CNFs supercapacitors employing (a) 1 M H2SO4, (b) 6 M KOH, (c) Dead Sea Water, and (d) conc. Dead Sea Water electrolytes at various scan rates

Scan rate (mV/s)	Cs (F/g)			
	1 M H2SO4	6 M KOH	Dead Sea water	Concentrated Dead Sea water
5	145.46	157.86	139.6	134.30
10	137.72	132.59	125.37	105.41
20	126.70	105.36	114.61	94.52
50	103.93	87.96	95.00	74.12
100	78.50	77.40	78.54	56.54
150	62.81	69.11	67.13	47.20

Table 4.1 reveals that while the scan rate increases, the specific capacitance decreases. This occurs because the ions have had sufficient time to grab and migrate into unoccupied pores. The widely accepted understanding is that at lower scan rates, C_S values are elevated due to the increased time available for ions to reach the accessible pores of the electrode and create the electric double layer (EDL) (14). Therefore, by maximizing the available surface area for ions, the capacitance of the capacitor is enhanced, and consequently, C_S increases. C_S for electrode with 1 M H_2SO_4 is shown to be greater than other electrolytes at higher scan rate (10, 20, 50 mV/s). Except for the electrode with concentrated Dead Sea water electrolytes, the C_s for all electrodes at scan rate (100 mV/s) are found to be almost equal, with specific capacitances (78.50, 77.40, 78.54 F/g) with 1 M H_2SO_4, 6 M KOH, and Dead Sea water, respectively.

The lowest C_S values were observed for concentrated Dead Sea water electrolytes. This decrease in C_S for electrodes with concentrated Dead Sea water electrolytes may be due to the presence of a complicated relationship between the ion mobility in the electrolyte and the ion concentration (67). As the concentration of ions increases, so do the particle-particle interactions, but the movement of free water molecules and salt ions is constrained by the presence of hydration and the formation of ion pairs (68). As ion concentrations increase, ion mobility decreases dramatically due to increased viscosity

(67). This is also due to the presence of ions with large hydrated ionic diameters like Mg^{+2}, Ca^{+2}, Na^{+}, and SO_4^{-2}); see Table 4.2, the effects of which increase with increasing Dead Sea water concentration.

When the ionic diameter of the ion in its hydrated form decreases, it will be able to penetrate deeper into the pores of the electrodes. Consequently, this will lead to an expansion of the specific surface area and, as a result, an increase in the specific capacitance, C_s. Table 4.2 shows the radii of non-hydrated and hydrated ions in used electrolytes and Dead Sea water.

Figure 4.3

Specific capacitance vs. scan rate for all samples

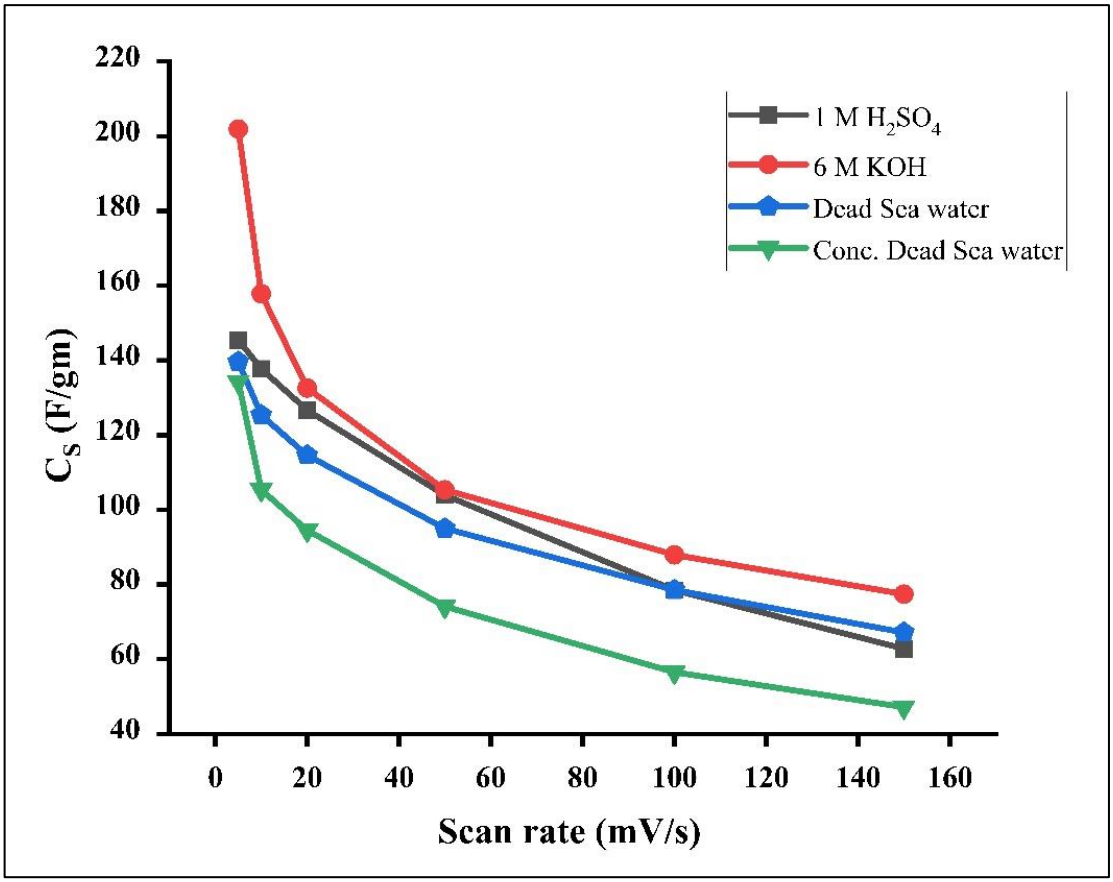

Because of the solvation energy, ions in an aqueous electrolyte have a solvent shell that remains intact as they enter the large pores. However, when the solvated ions enter nanopores, they may desolvate or distort. The diameter of non-solvated ions in the 6 M KOH aqueous electrolyte utilized in the cell system is 0.28 nm for K^+ and 0.298 nm for OH^-, whereas the effective diameter of the solvated ions is 0.66 nm for K^+ and 0.60 nm

for OH^- (62). The diameter of non-solvated ions in the 1 M H_2SO_4 aqueous electrolyte used in the cell system is 0.06 nm for H^+ and 0.46 nm for SO_4^{-2}, whereas the effective diameter of the solvated ions is 0.56 nm for H^+, which exists as hydronium ion (H_3O^+) in the aqueous solution (69), and 0.76 nm for SO_4^{-2}. The smaller the size of the ions, the greater the degree of hydration. Thus, H^+ ions get much more hydrated than K^+ ions. Because of the increased hydration radius, ion adsorption at the electrode/electrolyte interface is constrained, affecting the specific capacitance value (70). Table 4.2 shows the radii of non-hydrated and hydrated ions in used electrolytes

Table 4.2

The radii of non-hydrated and hydrated ions in used electrolytes

Ion	Non-hydrated ionic radius (nm)	Hydrated ionic radius (nm)	Reference
K^+	0.138	0.331	(70)
OH^-	0.133	0.300	(70)
H^+	0.030	0.282	(70)
SO_4^{-2}	0.230	0.379	(70)
Cl^-	0.181	0.270	(47)
Mg^{+2-}	0.078	0.395	(47)
Na^+	0.098	0.360	(47)
Ca^{+2}	0.106	0.348	(47)

Due to the importance of cyclic stability in practical applications, the cyclic stability of the AC/CNFs composite electrode was investigated for all electrolytes used. As shown, all samples have extremely good cycle stability. The cyclic stability of 1 M H_2SO_4, 6 M KOH, Dead Sea water, and concentrated Dead Sea water electrolytes is shown Figure (4.4. a–d) from the first to the hundredth cycle. All the one hundred cycles for all electrolytes had the same form as the initial cycle, demonstrating that the four electrolytes have great reversibility and good stability.

Figure 4.4

Cyclic stability at scan rate =100 mV for AC/CNFs supercapacitor for the first 100 cycle

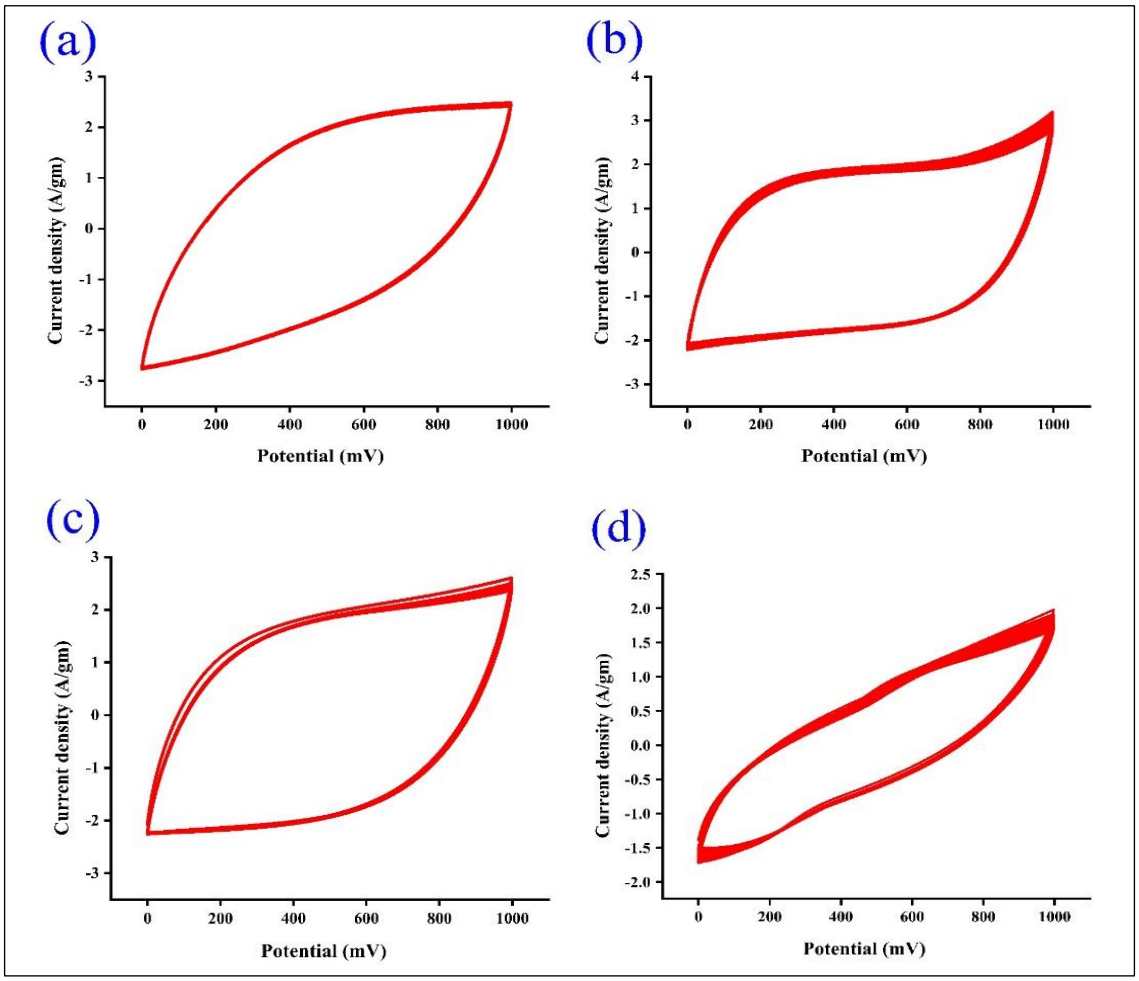

(a) 1 M H_2SO_4, (b) 6 M KOH, (c) Dead Sea Water, (d) concentrated Dead Sea water electrolytes.

4.1.2 Galvanostatic charge-discharge (GCD)

The specific capacitance was determined for various current density values, representing the current per unit mass of the electrode (I/m in A/g). Figure 4.5 (a-d) illustrates the relationship between potential and the time needed for both charging and discharging processes for the four examined electrolytes.

Figure 4.5

Galvanostatic charge-discharge curves for AC/CNFs supercapacitors at currents ranging from 10 to 150 mA

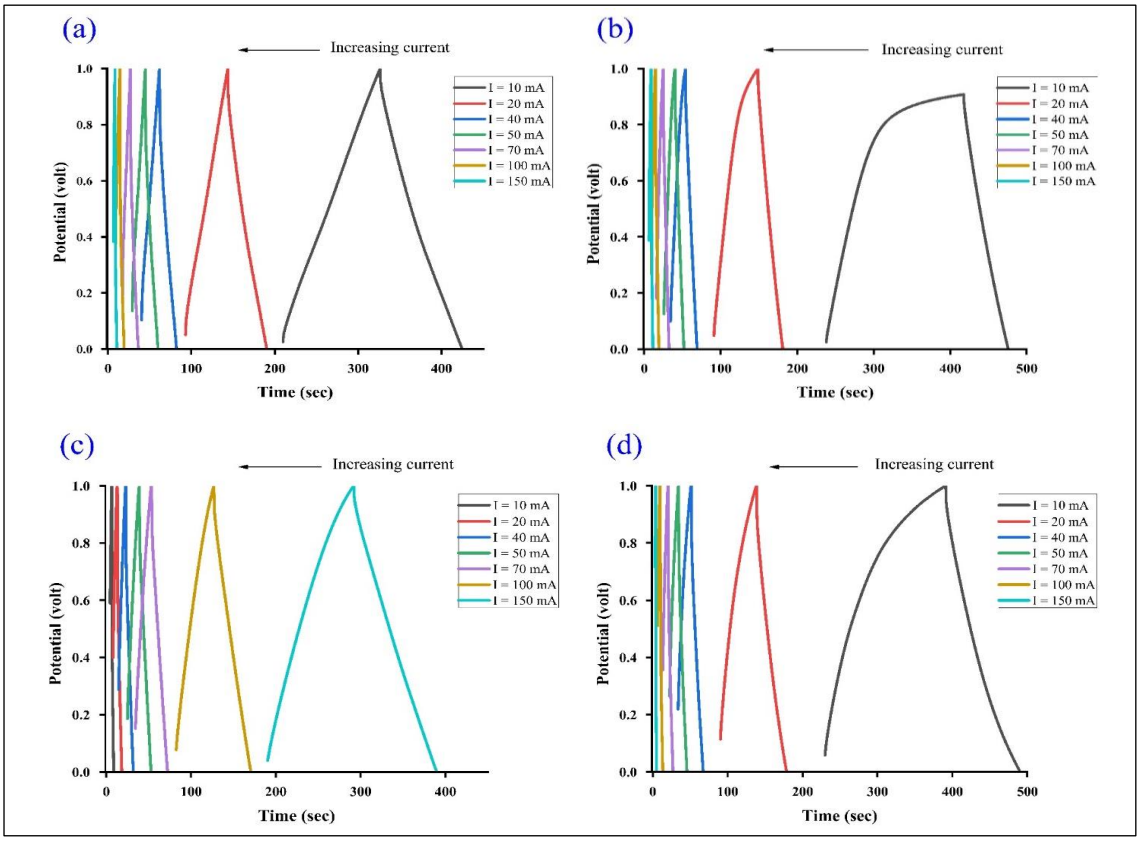

(a) 1 M H_2SO_4, (b) 6 M KOH, (c) Dead Sea Water, (d) conc. Dead Sea water electrolytes.

Figure 4.6 illustrates a comparison analysis of the four samples at a current of 40 mA. The calculation of specific capacitance was carried out for various current densities using equation 2.9, and the findings have been summarized in Table 4.3 and illustrated in Fig. 4.6. As indicated in Table 4.3 and depicted in Fig. 4.6, there is an observable decline in specific capacitance as the current density increases. This is typically attributed to a limitation in ion diffusion within the electrode pores resulting from enhanced ion mobility at higher currents (15, 18, 37). The results show that the supercapacitor with concentrated Dead Sea water electrolyte has the highest C_S of 84.40 F/g at a low current density (I/m) of 0.4 A/g, while the supercapacitor with 6 M KOH electrolyte has the lowest Cs of 52.40 F/g at the same current density. By comparing the supercapacitors with each other, the electrodes with 1 M H_2SO_4, Dead Sea water, and concentrated Dead Sea water electrolyte have nearly similar Cs values of 81.22, 81.49, and 84.40 F/g, respectively, at low current densities (0.4 A/g). As previously stated, ionic liquids with the smallest ion radius and mass (H^+) have the largest specific capacitance. As the ionic

radius falls, it penetrates deeper into the electrode pores, resulting in a greater specific surface area (13, 18, 19).

Table 4.3

Specific capacitance utilizing GCD for various electrolytes at each current density (I/m)

	1 M H_2SO_4	6 M KOH	Dead Sea water	Conc. Dead Sea water
I/m (A/g)	Cs (F/g)	Cs (F/g)	Cs (F/g)	Cs (F/g)
0.4	81.22	52.40	81.49	84.40
0.8	78.74	54.51	74.505	69.64
1.6	72.95	53.17	68.34	61.02
2.0	70.10	52.40	67.31	57.84
2.8	64.89	49.97	64.10	53.10
4.0	55.76	46.56	60.84	45.51
6.0	40.17	42.82	53.87	37.50

As depicted in Table 4.3, the specific capacitance declines as the current density rises. This is attributed to the fact that elevated current densities impede the smooth diffusion and transfer of ions. Additionally, higher densities of current increase the potential for electrode material damage due to intensified electric fields. Consequently, the efficient retention of charges decreases as current density increases (71). Also, the reason may be that the interfacial electrolytes absorbed a large amount of electrolyte ions, the concentration of electrolyte ions at the interface declined quickly, and polarization increased (72).

Figure 4.6

Galvanostatic charge-discharge curves for comparison at specific current (I = 40 mA) of different aqueous electrolytes for such nanocomposite electrodes (AC/CNFs)

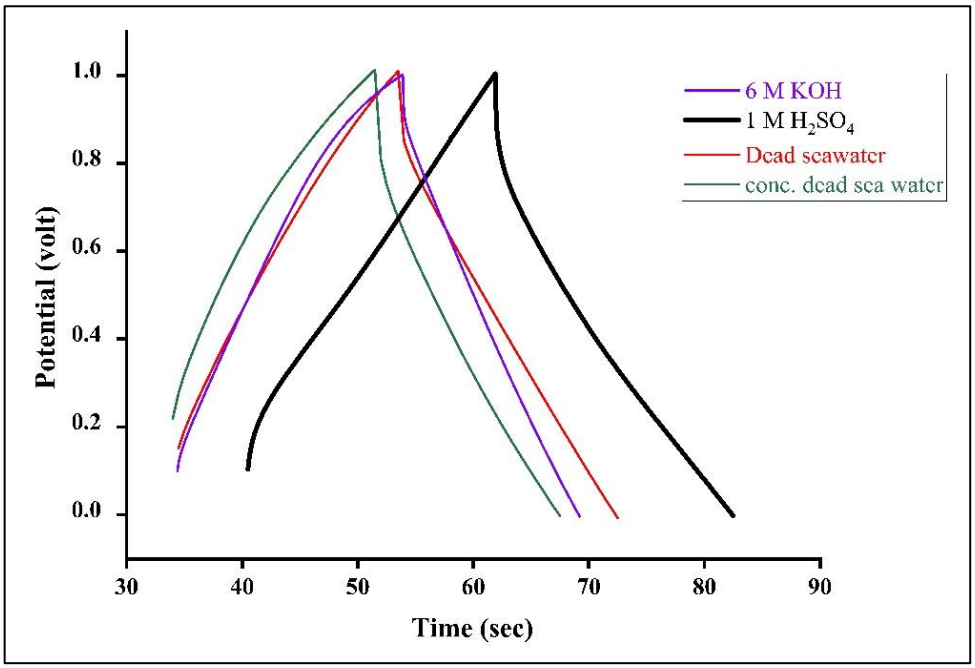

Figure 4.7

Variation of specific capacitance with current density for AC/CNFs electrodes in different electrolytes

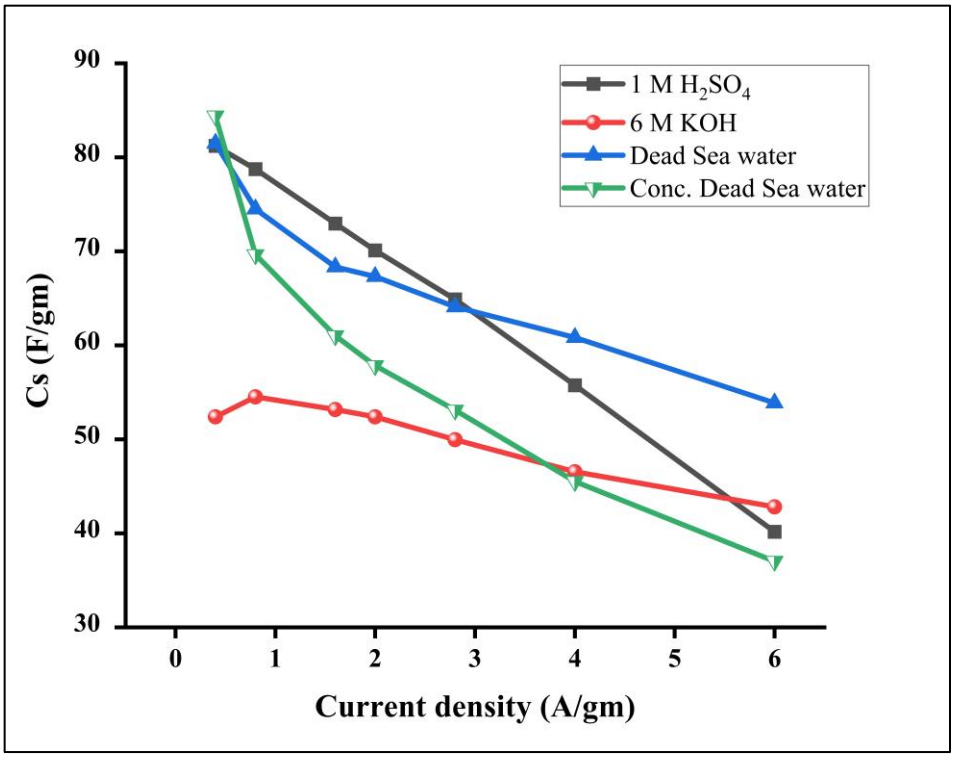

The voltage drop (V_{drop}) observed when transitioning from charging current (+I) to discharging current (-I) is generated by the ESR of the supercapacitor. The Vdrop attributed to potential losses due to the ESR of the composite electrode AC/CNFs was determined using GCD measurements. This analysis was conducted for all electrodes across various current densities.

Table 4.4

Voltage drop at each current density (I/m) using GCD for different electrolytes

	1 M H_2SO_4	6 M KOH	Dead Sea water	Conc. Dead Sea water
I/m (A/g)	V_{drop} (V)	V_{drop} (V)	V_{drop} (V)	V_{drop} (V)
0.4	0.0336	0.0265	0.0527	0.0666
0.8	0.0633	0.0575	0.0853	0.0994
1.6	0.1070	0.0800	0.1434	0.1918
2.0	0.1433	0.1198	0.1979	0.2518
2.8	0.2043	0.1540	0.2638	0.3470
4.0	0.2870	0.2210	0.3617	0.4880
6.0	0.4130	0.3490	0.5893	0.6970

Figure 4.8

Voltage drop vs. current density for AC/CNFs electrodes in different electrolytes

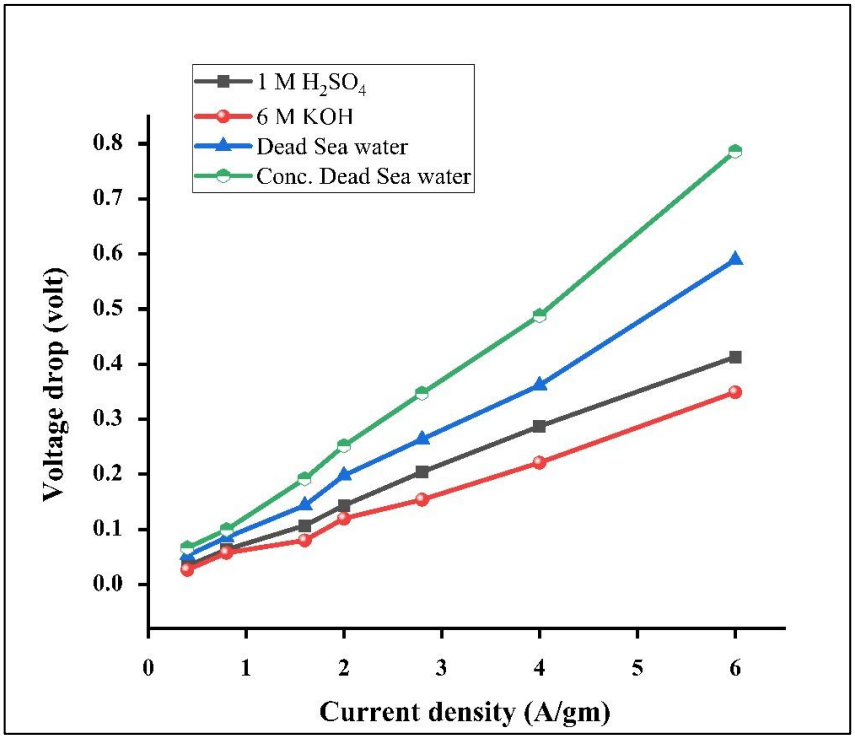

As seen in Table 4.4 and Fig. 4.8, all electrodes with different electrolytes showed an increasing voltage drop with increasing current density. By comparing Figs. 4.7 and (4.8), it can be deduced that as the charge-discharge current increases, the voltage drop increases and the capacitance decreases. This is due to an increase in the mobility of ions and, consequently, a drop in the conductivity of ions across the electrolyte (13, 19).

The calculated highest specific capacitance for a supercapacitor with Dead Sea water is 81.49 F/g at 0.4 A/g and decreases to 53.87 F/g at the current density of 6.0 A/g. It demonstrates that an AC/CNFs electrode with Dead Sea water reserves a higher capacitance even at a higher current density, meaning that it was the least affected by the increase in current density.

As shown in Table 4.5, the AC/CNFs electrode with 6 M KOH electrolyte has the lowest ESR. Furthermore, employing the 6 M KOH electrolyte charging curve, the AC/CNFs electrode exceeds the electrolyte stability window, as illustrated in Fig. 4.5.(b), resulting in excess charge transfer. As seen in Fig. 4.5.(a), the electrode with 1 M H_2SO_4 electrolyte exhibited a more symmetrical charge discharge curve, indicating that it has a low ESR, stronger conductivity, and superior electrochemical reversibility than other electrodes (13, 19).

For all developed electrodes ESR was determined from the slope of the V_{drop} vs. current density graph in Fig. 4.8, which corresponds to Eq. 2.12, and their values are presented in Table 4.5.

Table 4.5

ESR values for AC/CNFs electrodes tested by GCD method under different electrolytes

Sample	ESR (ohm)
1 M H_2SO_4	1.37
6 M KOH	1.13
Dead Sea water	1.89
Concentrated Dead Sea water	2.57

The supercapacitor electrode tested with 6 M KOH electrolyte has the lowest ESR when compared to those tested with 1 M H_2SO_4, Dead Sea water, and concentrated Dead Sea water. Also as expected, the electrode tested with 1 M H_2SO_4 has low ESR.

During the supercapacitor's discharging process, the energy density (E_d) and power density (P_d) of the prepared electrodes were determined using equations 2.10 and 2.11, respectively. The values of E_d and P_d for the four electrolytes at various discharge currents are shown in Table 4.6 in Appendix B.

To facilitate comparison between widely manufactured supercapacitor electrodes, the relation between P_d and E_d for an AC/CNFs composite electrode using the four different electrolytes was plotted (Ragone plot) and is shown in Fig. 4.9.

Figure 4.9

Energy density and power density relations for the AC/CNFs electrodes in different electrolytes

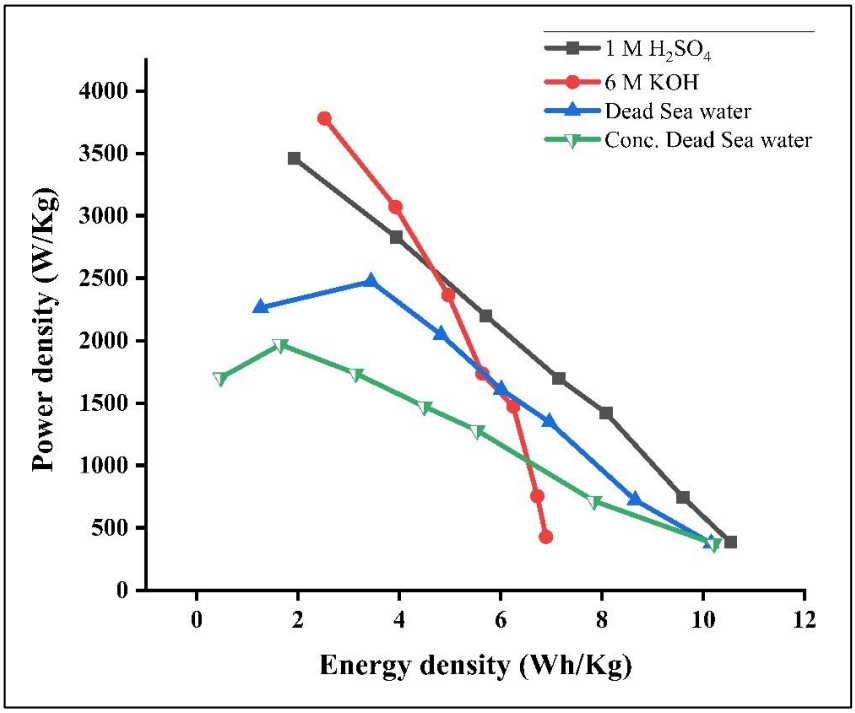

Fig. 4.9 shows the inverse relationship between energy density and power density, with an increase in energy density accompanied by a decrease in power density. This is expected behavior, as a decrease in power density normally lengthens the time required to deliver the energy stored in the device (19). Therefore, a device with a high energy density but a low power density can perform work for a relatively long period of time (73).

The AC/CNFs composite electrode using H_2SO_4 electrolyte was found to have the highest power and energy densities at discharge currents greater than 0.02 A, as shown in Table 4.6 in Appendix B and Fig. 4.9. It has a power density that increases from 385.43 to 3460.33 W/Kg and energy density decreases from 10.535 to 1.922 Wh/Kg, while the supercapacitor with 6 M KOH electrolyte has the lowest ESR and the highest power density at discharge currents less than 0.04 A.

The GCD technique was used to assess the cyclic satiability of all constructed electrodes at a current value of 100 mA. For the first 200 cycles, C_S drops to 99.5%, 99.6%, 99.3%, and 99.8% for supercapacitor electrodes with concentrated Dead Sea water, 1 M H_2SO_4, 6 M KOH, and Dead Sea water, respectively, as shown in Fig. 4.10 in Appendix A. Across the entire cycle number range, all electrodes consistently demonstrate remarkable stability. This exceptional stability emphasizes the suitability of these electrodes for use in supercapacitors, ensuring extended cycling lives.

4.1.3 Electrochemical Impedance Spectroscopy (EIS)

The electrochemical impedance spectroscopy (EIS) method was used to investigate the impedance of a supercapacitor cell when an alternating current (AC) signal with different input frequencies was applied. Each cell was subjected to a 20-mV-amplitude AC sine wave with frequency ranges ranging from 10 mHz to 100 kHz.

EIS is frequently illustrated by the Nyquist plot, which shows the real and imaginary components of the impedance on both the x and y axes. The Nyquist plot takes into consideration various factors, like capacitance, resistance, inductance, and so on, that are all frequency dependent (74). The Nyquist plot schematic in Fig. 2.10 in Appendix A is obtained using electrochemical impedance spectroscopy. In the low-frequency range, the specific capacitance can be calculated depending on the imaginary component of impedance in Equation 2.16. In the high-frequency domain, the solution resistance (R_A), charge transfer resistance (R_{AB}), and consequently, the ESR are determined by analyzing where the semicircle intersects the real component of the impedance (59).

The Nyquist curve for a frequency range of 10 mHz-100 kHz for AC/CNFs supercapacitor electrodes investigated using 1 M H_2SO_4, 6 M KOH, Dead Sea water, and concentrated Dead Sea water electrolytes is shown in Fig. 4.11 in Appendix A. The Cs value for composite electrodes has been demonstrated to be substantially depends on the

frequency of the applied voltage. As predicted, the imaginary component of impedance decreases with increasing frequency in all samples. The semicircle diameter (R_{AB}) observed in the Nyquist plot at high frequencies was found to begin at the lowest value of the impedance real point. The radius of the semicircle ($= R_{AB}/2$) indicates the polarization resistance (R_P) and provides information on the accessibility of the electrolyte in the pores.

The values of specific capacitance, solution resistance (R_A), charge transfer resistance (R_{AB}), and equivalent series resistance (ESR) at 10 mHz frequency for AC/CNF composite electrodes using various electrolytes were determined and illustrated in Table (4.7).

Table 4.7

The results of the EIS technique of specific capacitance (C_s), solution resistance (R_A), charge transfer resistance (R_{AB}), and equivalent series resistance (ESR) at 10 mHz frequency for AC/CNF composite electrodes with different electrolytes

Electrolyte	C_s (F/g)	ESR (Ω)	R_A (Ω)	R_{AB} (Ω)
1 M H_2SO_4	150.32	0.9	0.8	0.1
6 M KOH	93.81	0.72	0.2	0.52
Dead Sea water	98.83	0.68	0.58	0.1
Conc. Dead Sea water	105.1	1.0	0.2	0.8

The specific capacitance for the AC/CNFs electrode with different electrolytes was 150.3, 105.1, 98.8, and 93.8 F/g for 1 M H_2SO_4, Conc. Dead Sea water, Dead Sea water, and 6 M KOH, respectively. The highest Cs was for 1 M H_2SO_4, while the lowest was for 6 M KOH. The variation in specific capacitance among the different electrolytes for the AC/CNFs electrode can be attributed to differences in electrolyte conductivity, composition, ion size, ion mobility, and electrolyte concentration. These factors collectively influence the charge storage capacity and performance of the electrode in each electrolyte solution. The size and mobility of ions in the electrolyte can play a role in determining the specific capacitance. Smaller and more mobile ions tend to diffuse more quickly to the electrode surface, leading to higher capacitance. Potassium ions (K^+) in KOH are relatively larger and less mobile compared to protons (H^+) in sulfuric acid, which might contribute to the lower specific capacitance observed with 6 M KOH. The

concentration of the electrolyte can also influence the specific capacitance. Extremely high concentrations of electrolyte might lead to increased ion crowding and limited access to the electrode surface, reducing capacitance.

Figure 4.12 in Appendix A shows the computed specific capacitance, C_S, for all samples in the selected frequency range. The graph demonstrates that all samples had an increase in C_S at low frequencies below 10 Hz. The frequency dispersion phenomenon explains this: a high-frequency voltage signal is difficult to enter within the small pores, but a low-frequency signal may easily penetrate the electrode's porous structure (19).

As seen in Fig. 4.12 in Appendix A, at low frequencies, samples investigated with H_2SO_4 electrolytes had a greater specific capacitance than samples tested with KOH, Dead Sea Water, or concentrated Dead Sea Water. This is due to the H^+ ion's lowest ionic radius in the H_2SO_4 electrolyte. In addition, electrodes with H_2SO_4 electrolytes have the lowest charge transfer resistance(R_{AB}), which leads to the highest ion conductivity.

The knee frequency f_0 represents the maximum frequency where capacitive behavior is predominance in the supercapacitor. Thus, for, $f < f_0$ the supercapacitor behaves as a pure capacitor, while for $f > f_0$, the supercapacitor behaves as a resistor (75). The knee frequency (f_0) was found and represented in Table 4.8 for all AC/CNFs electrodes at a point where the imaginary part of the impedance rapidly increased in the Nyquist plot.

Table 4.8

Knee frequency for the prepared supercapacitors using different electrolytes

Sample	f_0 (mHz)
1 M H_2SO_4	71
6 M KOH	79
Dead Sea water	79
Concentrated Dead Sea water	125

The electrode with concentrated Dead Sea water electrolyte has the greatest knee frequency (f_0= 0.125 Hz), followed by the electrode with 6 M KOH and electrode with Dead Sea water electrolytes, both of which have (f_0= 0.079 Hz). The lowest f_0(0.071 Hz) is for the electrode with 1 M H_2SO_4 electrolyte.

The highest knee frequency (f_0) implies a rapid rate of transfer from resistive to capacitive behavior, which is ideal for the supercapacitor. In supercapacitor applications where perfect capacitance is required, the maximum operating frequency is constrained by f_0 (18, 19). Consequently, active materials used in electrochemical capacitor applications should have a high knee frequency (75).

At the lowest frequency of 0.01 Hz, the time constant for AC/CNFs composite electrodes using different electrolytes was calculated using Eq. (2.18), and the results are represented in Table 4.9. This constant is an indicator of how fast the charge transfer process is (76). A supercapacitor with a short time constant has a high response rate (19).

The electrode with Dead Sea water electrolyte has the lowest time constant (τ = 1.68 sec), followed by the electrode with 6 M KOH electrolyte (τ = 1.69 sec), which is almost equal to that with Dead Sea water. The electrode with 1 M H_2SO_4 electrolyte has the highest value (τ = 3.38 sec), while the electrode with concentrated Dead Sea water has a moderate value (τ = 2.63 sec).

Table 4.9

Time constant (τ) and relaxation time (τ_0) for the prepared supercapacitors using different electrolytes

Sample	τ (sec)	τ_0 (sec)
1 M H_2SO_4	3.38	14.1
6 M KOH	1.69	12.7
Dead Sea water	1.68	12.7
Concentrated Dead Sea water	2.63	8.0

The relaxation time values of the supercapacitors with various electrolytes were determined from the knee frequency using Eq. 2.17, and the results are shown in Table 4.9. Relaxation time presents the shifting of an electrochemical capacitor from resistive to capacitive behavior (76). Concentrated Dead Sea water had the shortest relaxation time (τ_0= 8.0 sec) followed by the electrode with 6 M KOH and electrode with Dead Sea water electrolytes, both of which have (τ_0= 12.7 sec). The electrode with 1 M H_2SO_4 electrolyte had the longest relaxation time (τ_0= 14.1 sec).

Short relaxation times are desired for effective power delivery in power devices since they indicate the shortest period of time required to discharge all of the energy from a device with an efficiency greater than 50% (18, 19, 76). The relationship between the real part of the impedance (Zr) and frequency, as shown in Fig. 4.13 in Appendix A, gives the equivalent series resistance (ESR) for the prepared AC/CNFs electrodes. The Z_r value increases significantly with decreasing frequency below f_0 and approaches zero with increasing frequency above f_0. This indicates that the SC behaves as a resistor at high frequencies and as a capacitor at low frequencies.

Lowering the frequency value extends the time required for ions to penetrate the pores. Consequently, more ions become engaged in the charge and discharge processes, facilitating the filling of certain pore types. However, some pores need additional time for ions to penetrate deeply, resulting in further charge migration and increasing the displacement and diffusion layers within the electrolyte. This, in turn, leads to a decrease in conductivity and an increase in ESR (60). The concentrated Dead Sea water sample exhibited the greatest resistance due to the reduced penetration of ions into the pores compared to the other samples.

While the relationship between the imaginary part of the impedance (Z_i) vs. frequency, as shown in Fig. 4.14 in Appendix A, informs us about the region where the supercapacitor switches from a resistive to a capacitive behavior.

The relationship between the imaginary portion of the impedance and frequency is depicted in Fig. 4.14 in Appendix A. The imaginary portion of the impedance diminishes until it hits zero at high frequencies, which reinforces the resistive behavior. As anticipated, the samples behave like an ideal capacitor: as the frequency value decreases, the imaginary part of the impedance increases in the negative direction until it reaches the value ($Z = \frac{1}{jwC}$). Below f_0, the value of Z_i dramatically increases, demonstrating capacitive behavior for the supercapacitor, while the Z_i predominates and approaches zero as frequency increases in the region of ($f > f_0$). The Z_i for 1 M H_2SO_4, 6 M KOH, D.S. water, and conc. D.S. water were (-0.28, -0.79, -0.31, -0.29) at 100 kHz and (-18.63, -27.15, -25.77, -24.24) at 0.01 Hz, respectively.

The imaginary part of the capacitance was plotted as a function of frequency (*C" vs. f*). Fig. 4.15 in Appendix A presents the evolution of this relation. The imaginary capacitance reaches a maximum at frequency f_0, defining a time constant as ($\tau_0 = {}^{1}/_{f_0}$) (77). The supercapacitor's capacitive behavior at the lower knee frequency is clearly shown in Fig. 4.15 in Appendix A.

The Bode plot, which is illustrated in Fig. 4.16 in Appendix A, shows how phase angle changes as a function of frequency. The phase angle increases with decreasing frequency. The phase angle should be close to zero for resistive behavior at high frequencies (60). Also, as the phase angle approaches -90°, this indicates better capacitive behavior and a fast charge-discharge cycle (18). The phase angles at 0.01 Hz frequency were ($-83.6^{\circ}, -80.7^{\circ}, -72.9^{\circ}, and\ -66.2^{\circ}$) for Dead Sea water, 6 M KOH, 1 M H_2SO_4, and concentrated D.S. water, respectively. These results are illustrated in Table 4.10 in Appendix B. This indicates that the prepared supercapacitor with Dead Sea water electrolyte has the best capacitive behavior and a fast charge-discharge cycle.

4.2 Morphology of the electrode surface

The physical surface morphology of AC, CNFs, and AC/CNFs composite electrodes was investigated using scanning electron microscopy (SEM) (JEOL J-7100) as shown in Figs. 4.17 (a), (b), and (c) in Appendix A, respectively. TEM images were attained by a JEOL 2011 electron microscope to define the interior structure of particles in a sample of 90% AC and 10% CNFs, as seen in Fig. 4.17(d) in Appendix A (18).

The surface morphology of AC/CNFs electrode indicates that the electrode material's surface shows a coarse and porous structure with differing particle sizes. Two types of grains are observed in SEM and TEM micrographs that correspond to CNFs fragments spread on AC particles. Treatment of AC with CNFs enhances its capacitance by enlarging the available surface area through the opening of closed or obstructed pores.

The electrode matter should possess a large surface area, high porosity, and extremely low electrical resistance for supercapacitor applications. The large surface area and many mesopore (2-50 nm) structures enable efficient passing of electrons and ions, which leads to a high electrochemical capacitance (18).

4.3 Porosity of AC/CNFs composite

When considering porosity, a general tendency toward greater capacitance is observed as the specific surface area (SSA) increases. Also, it's important to consider other factors related to the carbon structure, such as pore shape, surface functional groups, and electrical conductivity. This can be done by treating the AC in several ways to improve its capacitance, including increasing the surface area and opening closed or obstructed pores (78).

Using the N_2 adsorption/desorption isotherm at a relative pressure P/P_0 of roughly 1, the porosity of the AC/CNFs composite electrode material was investigated using a Brunauer-Emmett-Teller analyzer (BET, TriStar 3000 V6.04A). The N_2 adsorption/ desorption isotherm for the AC/CNFs composite electrode is shown in Fig. 4.18 in Appendix A.

As illustrated in Fig. 4.18 in Appendix A, as the relative pressure rises, more gas is absorbed into the pores of the material, filling all of them up at a relative maximum pressure of almost 1. The amount of N_2 absorbed at maximum relative pressure was 398.2 cm^3/g STP, and the total specific pore volume (V_{tot}) for the electrode material was 0.693 cm^3/g. Very strong absorption of N_2 was detected at very low relative pressures ($P/P_0 < 0.01$), pointing to the presence of many micropores in the material of the electrode. The presence of capillary condensation within the mesopores is responsible for the hysteresis loop observed at elevated relative pressures ($P/P_0 > 0.5$).

As shown in Fig. 4.18 in Appendix A, over the range of the relative pressure for the N_2 adsorption/desorption loop, the branches stay essentially horizontal and parallel (almost identical). This behavior is frequently associated with small, slit-like pores with high microporosity (18). According to the IUPAC classification, the isotherm depicted in Fig. 4.18 in Appendix A is a form of type IV-H4 physical adsorption isotherm.

4.4 Specific surface area (SSA)

Using nitrogen multilayer adsorption isotherms, BET analysis is used to evaluate the total specific surface area of materials by measuring both the external area and pore area, typically expressed in units of square meters per gram (m^2/g). The Brunauer-Emmett-Teller (BET) method had been used to investigate the total specific surface area (S_{BET}) of AC/CNFs composite in relative pressure range of 0.006 to 0.20. From the linear BET plot shown in Fig. 4.19 in Appendix A, S_{BET} was taken out, which is accessible for electrolyte ions.

Table 4.11 in Appendix B displays the BET plot's findings together with the supplied data. Although the total specific pore volume was small (0.693 cm^3/g), the specific surface area considerably large (962.06 m^2/g). When utilized with various electrolytes using the CV method at a scan rate of 5 mV/s, it was found that the prepared AC/CNFs composite had a high specific capacitance. The high capacitance of the prepared AC/CNFs composite is attributed to its wide specific surface area and high porosity, which highlights the possibility of its use in the manufacture of supercapacitors.

Chapter Five

Conclusions

Each supercapacitor electrode, which was made up of 90% AC and 10% CNFs, was investigated using a glass fiber separator with a variety of electrolytes (6 M KOH, 1 M H_2SO_4, and various concentrations of Dead Sea water). The cyclic voltammetry (CV) response of the electrodes was tested at different scan speeds that range from 5 to 150 mV/s. At a 100 mV/s scan rate, the area inside the CV curve was the same for electrodes with 1 M H_2SO_4, 6 M KOH, and Dead Sea water electrolytes. This means that the electrodes had similar amounts of stored charges and, therefore, similar specific capacitance (C_S). However, the area inside the CV curve for electrodes with concentrated Dead Sea water electrolytes was the smallest. This means that the electrodes had the lowest stored charges and thus the smallest C_S. The C_S for electrodes with 6 M KOH was found to be slightly greater than that for other electrolytes at a 5 mV/s scan rate, with a maximum specific capacitance of 157.86 F/g at the same scan rate. The results reveal that while the scan rate increases, the specific capacitance decreases. The C_S for electrode with 1 M H_2SO_4 is shown to be greater than other electrolytes at higher scan rate (10, 20, 50 mV/s). Except for the electrode with concentrated Dead Sea water electrolytes, the Cs for all electrodes at scan rate (100 mV/s) are found to be almost equal, with specific capacitances (78.50, 77.40, 78.54 F/g) with 1 M H_2SO_4, 6 M KOH, and Dead Sea water, respectively. The lowest C_S values were observed for concentrated Dead Sea water electrolytes. This decrease in C_S for electrodes with concentrated Dead Sea water electrolytes may be due to the presence of a complicated relationship between the ion mobility in the electrolyte and the ion concentration. The cyclic stability of 1 M H_2SO_4, 6 M KOH, Dead Sea water, and concentrated Dead Sea water electrolytes is shown in Figure 4.4(a-d) from the first to the hundredth cycle. All the one hundred cycles for all electrolytes had the same form as the initial cycle, demonstrating that the four electrolytes have great reversibility and good stability.

The GCD studies were carried out with currents ranging from 10 to 150 mA. The results show that the specific capacitance decreases with increasing current density. The results show that the supercapacitor with concentrated Dead Sea water electrolyte has the highest C_S of 84.40 F/g at a low current density (I/m) of 0.4 A/g, while the supercapacitor with 6 M KOH electrolyte has the lowest C_S of 52.40 F/g at the same current density. By

comparing the supercapacitors with each other, the electrodes with 1 M H_2SO_4, Dead Sea water, and concentrated Dead Sea water electrolyte have nearly similar C_S values of 81.22, 81.49, and 84.40, respectively, at low current densities (0.4 A/g). All of the electrodes with different electrolytes showed a drop in voltage as the current density increases. This is due to the increase of the ions' mobility, which causes the conductivity of the ions across the electrolyte to drop. The calculated highest specific capacitance for a supercapacitor with Dead Sea water is 81.49 F/g at 0.4 A/g and decreases to 53.87 F/g at the current density of 6.0 A/g. It demonstrates that an AC/CNFs electrode with Dead Sea water reserves a higher capacitance even at a higher current density, meaning that it has the least effect on the increase in current density. The AC/CNFs electrode with 6 M KOH electrolyte has the lowest ESR. Furthermore, employing the 6 M KOH electrolyte charging curve, the AC/CNFs electrode exceeds the electrolyte stability window resulting in excess charge transfer. As seen in Fig. 4.5(a), the electrode with 1 M H_2SO_4 electrolyte exhibited a more symmetrical charge discharge curve, indicating that it has a low ESR, stronger conductivity, and superior electrochemical reversibility than other electrodes. The supercapacitor electrode tested with 6 M KOH electrolyte has the lowest ESR when compared to those tested with 1 M H_2SO_4, Dead Sea water, and concentrated Dead Sea water. Also as expected, the electrode tested with 1 M H_2SO_4 has low ESR. AC/CNFs composite electrode using 1 M H_2SO_4 electrolyte was found to have the highest power and energy densities at discharge currents greater than 0.02 A. It has a power density that increases from 385.43 to 3460.33 W/Kg and an energy density that decreases from 10.535 to 1.922 Wh/Kg. All electrodes exhibit high stability with cycle number. This high stability indicates that these electrodes are suitable to be used as supercapacitors with long cycling lives.

The electrochemical impedance spectroscopy (EIS) method was used to investigate the impedance of a supercapacitor cell when an alternating current (AC) signal with different input frequencies was applied. Each cell was subjected to a 20-mV-amplitude AC sine wave with frequency ranges ranging from 10 mHz to 100 kHz. The Nyquist plot was utilized to analyze the frequency response of AC/CNFs supercapacitor electrodes within the frequency range of 10 mHz to 100 kHz. This investigation involved the use of four different electrolytes, namely 6 M KOH, 1 M H_2SO_4, Dead Sea water, and concentrated Dead Sea water. The values of specific capacitance, equivalent series resistance (ESR),

solution resistance (R_A), and charge transfer resistance (R_{AB}) at 10 mHz frequency for AC/CNFs composite electrodes using different electrolytes are determined and illustrated in Table 4.7. The specific capacitance values for the AC/CNFs electrode with different electrolytes were 150.3, 105.1, 98.8, and 93.8 F/g for 1 M H_2SO_4, Conc. Dead Sea water, Dead Sea water, and 6 M KOH, respectively. The highest C_S was for 1 M H_2SO_4, while the lowest was for 6 M KOH.

The electrode with concentrated Dead Sea water electrolyte has the greatest knee frequency (= 0.125 Hz), which implies a rapid rate of transfer from resistor to capacitor behavior, which is ideal for the supercapacitor. It is followed by the electrode with 6 M KOH and the electrode with Dead Sea water electrolytes, both of which have (= 0.079 Hz). The lowest (= 0.071 Hz) is for the electrode with 1 M H_2SO_4 electrolyte. At the lowest frequency of 0.01 Hz, the time constant for AC/CNFs composite electrodes using different electrolytes was calculated. The electrode with Dead Sea water electrolyte has the lowest time constant (τ = 1.68 sec), followed by the electrode with 6 M KOH electrolyte (τ = 1.69 sec), which is almost equal to that with Dead Sea water. The electrode with 1 M H_2SO_4 electrolyte has the highest value (τ = 3.38 sec), while the electrode with concentrated Dead Sea water has a moderate value (τ = 2.63 sec). The relaxation times of the supercapacitors with various electrolytes were determined from the knee frequency. Concentrated Dead Sea water had the shortest relaxation time (τ_0= 8.0 sec), which is desired for effective power delivery in power devices, followed by the electrode with 6 M KOH and electrode with Dead Sea water electrolytes, both of which have (τ_0= 12.7 sec). The electrode with 1 M H_2SO_4 electrolyte had the longest relaxation time (τ_0= 14.1 sec). The imaginary part of the impedance (Z_i) for 1 M H_2SO_4, 6 M KOH, D.S. water, and conc. D.S. water were (-0.28, -0.79, -0.31, -0.29) at 100 kHz and (-18.63, -27.15, -25.77, -24.24) at 0.01 Hz, respectively. The phase angles at 0.01 Hz frequency were ($-83.6^{\circ}, -80.7^{\circ}, -72.9^{\circ}, and\ -66.2^{\circ}$) for Dead Sea water, 6 M KOH, 1 M H_2SO_4, and concentrated D.S. water, respectively. The AC/CNFs electrode with Dead Sea water indicates better capacitive behavior and a fast charge-discharge cycle as its phase angle approaches -90°.

The surface morphology of AC/CNFs electrode indicates that the electrode material's surface shows a coarse and porous structure with differing particle sizes. Two types of grains are observed in SEM and TEM micrographs that correspond to CNFs fragments spread on AC particles. The treatment of AC with CNFs increases the capacitance of AC by increasing the surface area by opening pores that are closed or obstructed.

The behavior of the AC/CNFs electrode was one that is typically seen in narrow, slit-like pores with high microporosity. This is confirmed by the results presented in Table 4.11 in Appendix B. According to the IUPAC classification, the isotherm depicted in Fig. 4.18 in Appendix A is a form of type IV-H4 physical adsorption isotherm.

The total specific pore volume was small (0.693 cm^3/g), but the specific surface area was considerable (962.06 m^2/g). When utilized with various electrolytes using the CV method at a scan rate of 5 mV/s, it was found that the prepared AC/CNFs composite had a high specific capacitance. This high capacitance is due to its large specific surface area and high porosity, which indicate that the prepared AC/CNFs composite is a promising candidate for supercapacitor applications.

List of Abbreviations

Symbol	Abbreviation
AC	Activated carbon
BET	Brunauer- Emmet- Teller
BJH	Barrett- Joyner- Halenda
C	Capacitance
C"	The imaginary part of the capacitance
CNFs	Carbon-Nanofibers
C_s	Specific capacitance
CV	Cyclic Voltammetry
D.S.	Dead Sea
E_d	Energy density
EDLC	Electric Double Layer Capacitor
EIS	Electrochemical Impedance Spectroscopy
ESR	Equivalent series resistance
f_0	Knee frequency
GCD	Galvanostatic Charging Discharging
IUPAC	International Union of Pure and Applied Chemistry
P_d	Power density
PSD	Pore size distribution
PTFE	Polytetrafluoroethylene
PVDC	Polyvynilidene chloride
PVDF	Polyvynilidene fluoride
Q_m	Adsorbed Quantity
R_A	Solution resistance
R_{AB}	Charge transfer resistance
R_p	Polarization resistance
S_{BET}	total specific surface area
SCs	Supercapacitors
SEM	Scanning electron microscope
SSA	Specific surface area
STP	Standard temperature & pressure
TEM	Transmission electron microscope
V_{drop}	Drop voltage
Z_i	Imaginary part of the impedance
Z_r	Real part of the impedance
τ	Time constant
τ_0	Relaxation time

References

1. Farma R, Deraman M, Talib I, Omar R, Manjunatha J, Ishak M, et al. Physical and electrochemical properties of supercapacitor electrodes derived from carbon nanotube and biomass carbon. International Journal of Electrochemical Science. 2013;8(1):257-73.

2. Aslani M. Electrochemical double layer capacitors (supercapacitors). Standford University. 2012.

3. Chen T, Dai L. Carbon nanomaterials for high-performance supercapacitors. Materials Today. 2013;16(7-8):272-80.

4. Pan H, Li J, Feng Y. Carbon nanotubes for supercapacitor. Nanoscale research letters. 2010;5:654-68.

5. Liu Y, Jiang SP, Shao Z. Intercalation pseudocapacitance in electrochemical energy storage: recent advances in fundamental understanding and materials development. Materials Today Advances. 2020;7:100072.

6. Lourenço L, Branco PC. Electric Energy Storage using Ionic Polymer Metal Composites: Towards a Flexible Ionic Polymer Metal Composite Capacitor for Low-power Devices. Ionic Polymer Metal Composites (IPMCs)2015. p. 286-333.

7. Béguin F, Presser V, Balducci A, Frackowiak E. Carbons and electrolytes for advanced supercapacitors. Advanced materials. 2014;26(14):2219-51.

8. Iro ZS, Subramani C, Dash S. A brief review on electrode materials for supercapacitor. Int J Electrochem Sci. 2016;1.43-10628:(12)1

9. Zhang Y, Shao D, Yan J, Jia X, Li Y, Yu P, et al. The pore size distribution and its relationship with shale gas capacity in organic-rich mudstone of Wufeng-Longmaxi Formations, Sichuan Basin, China. Journal of Natural Gas Geoscience. 2.20-213:(3)1;016.

10. Borenstein A, Hanna O, Attias R, Luski S, Brousse T, Aurbach D. Carbon-based composite materials for supercapacitor electrodes: a review. Journal of Materials Chemistry A. 2017;5(25):12653-72.

11. Pandolfo AG, Hollenkamp AF. Carbon properties and their role in supercapacitors. Journal of power sources. 2006;157(1):11-27.

12. Sun X, Zhang X, Zhang H, Zhang D, Ma Y. A comparative study of activated carbon-based symmetric supercapacitors in Li 2 SO 4 and KOH aqueous electrolytes. Journal of Solid State Electrochemistry. 2012;16:2597-603.

13. Daraghmeh A, Hussain S, Saadeddin I, Servera L, Xuriguera E, Cornet A, et al. A study of carbon nanofibers and active carbon as symmetric supercapacitor in aqueous electrolyte: a comparative study. Nanoscale research letters. 2017;12:1-10.

14. Daraghmeh A, Hussain S, Haq AU, Saadeddin I, Servera L, Ruiz J. Carbon nanocomposite electrodes for electrical double layer capacitor. Journal of Energy Storage. 2020;32:101798.

15. Daraghmeh A, Hussain S, Servera L, Xuriguera E, Cornet A, Cirera A. Impact of binder concentration and pressure on performance of symmetric CNFs based supercapacitors. Electrochimica Acta. 2017;245:531-8.

16. Ruiz V, Blanco C, Granda M, Menéndez R, Santamaría R. Influence of electrode preparation on the electrochemical behaviour of carbon-based supercapacitors. Journal of applied electrochemistry. 2007;37:717-21.

17. Zhang S, Pan N. Supercapacitors performance evaluation. Advanced Energy Materials. 2015;5(6):1401401.

18. Daragmeh A .Advances in carbon nanofiber-based supercapacitors. 2017.

19. شحروج، محمد فن. Study of Active-Carbon (AC)/Graphene-Nanoplates as Supercapacitor Electrodes Using H2SO4, Na2SO4 and KOH Aqueous Electrolytes: An-Najah National University; 2021.

20. Holla S ,Selvakumar M. Effect of different electrolytes on the supercapacitor behavior of single and multilayered electrode materials based on multiwalled carbon nanotube/polyaniline composite. Macromolecular Chemistry and Physics. 2018;219(21):1800213.

21. Samsudin NA, Lim Y-C, Chang S-K, Heng I, Low FW, Shakeri M, et al. Titanium Dioxide Nanostructured Based Supercapacitors. 2022.

22. Joshi P, Sutrave D. Supercapacitor: basics and overview. J Inf Comput Sci. 2019; 9:12.

23. Yaseen M, Khattak MAK, Humayun M, Usman M, Shah SS, Bibi S, et al. A review of supercapacitors: materials design, modification, and applications. Energies. 2021;14(22):7779.

24. Winter M, Brodd RJ. What Are Batteries, Fuel Cells, and Supercapacitors? Chemical Reviews. 2004;104(10):4245-70.

25. Kumari P, Shandilya M, Lal M, Rai R. High dielectric materials for supercapacitors. Smart materials for smart living. 2017:95.

26. Conway B, Conway B. Energy Density and Power Density of Electrical Energy Storage Devices. Electrochemical Supercapacitors :Scientific Fundamentals and Technological Applications. 1999:417-77.

27. Iqbal MZ, Aziz U. Supercapattery: Merging of battery-supercapacitor electrodes for hybrid energy storage devices. Journal of Energy Storage. 2022;46:103823.

28. Sahin ME, Blaabjerg F, Sangwongwanich A. A review on supercapacitor materials and developments. Turkish Journal of Materials. 2020;5(2):10-24.

29. Castro-Gutiérrez J, Celzard A, Fierro V. Energy storage in supercapacitors: Focus on tannin-derived carbon electrodes. Frontiers in materials. 2020;7:217.

30. Gidwani M, Bhagwani A, Rohra N. Supercapacitors: the near future of batteries. International Journal of Engineering Inventions. 2014;4(5):22-7.

31. Solutions TG-C-dP. Ultracapacitors: Tecate Group; 2022 [Available from: https://www.tecategroup.com/products/ultracapacitors/ultracapacitor-FAQ.php#What_is_an_ultracapacitor.

32. Wayu M. Manganese oxide carbon-based nanocomposite in energy storage applications. Solids. 2021;2(2):232-48.

33. Tshiani C. The characterization of the electric double layer capacitor (EDLC) and its application in micro grids using the hybrid energy storage system (HESS).

34. Zhang LL, Zhao X. Carbon-based materials as supercapacitor electrodes. Chemical society reviews. 2009;38(9):2520-31.

35. Aqel A, Abou El-Nour KM, Ammar RA, Al-Warthan A. Carbon nanotubes, science and technology part (I) structure, synthesis and characterisation. Arabian Journal of Chemistry. 2012;5(1):1-23.

36. Carbotecnia. What is activated carbon and what is it used for? : Carbotecnia; 2022 [Available from: https://www.carbotecnia.info/learning-center/activated-carbon-theory/what-is-activated-carbon/?lang=en#que-es-el-carbon-activado.

37. Cheng Q, Tang J, Ma J, Zhang H, Shinya N, Qin L-C. Graphene and carbon nanotube composite electrodes for supercapacitors with ultra-high energy density. Physical Chemistry Chemical Physics. 2011;13(39):17615-24.

38. De Jong KP, Geus JW. Carbon nanofibers: catalytic synthesis and applications. Catalysis Reviews. 2000;42(4):481-510.

39. Mohamed A .Synthesis, characterization, and applications carbon nanofibers. Carbon-based nanofillers and their rubber nanocomposites: Elsevier; 2019. p. 243-57.

40. Ruiz-Cornejo JC, Sebastián D, Lázaro MJ. Synthesis and applications of carbon nanofibers: a review .Reviews in Chemical Engineering. 2020;36(4):493-511.

41. Pal B, Yang S, Ramesh S, Thangadurai V, Jose R. Electrolyte selection for supercapacitive devices: a critical review. Nanoscale Advances. 2019;1(10):3807-35.

42. Iqbal MZ, Zakar S, Haider SS. Role of aqueous electrolytes on the performance of electrochemical energy storage device. Journal of Electroanalytical Chemistry. 2020;858:113793.

43. Zhong C, Deng Y, Hu W, Qiao J, Zhang L, Zhang J. A review of electrolyte materials and compositions for electrochemical supercapacitors. Chemical Society Reviews. 2015;44(21):7484-539.

44. Scibioh MA, Viswanathan B. Chapter 4 - Electrolyte materials for supercapacitors. In: Scibioh MA, Viswanathan B, editors. Materials for Supercapacitor Applications: Elsevier; 2 .020p. 205-314.

45. Habib IM, El-Kelani RJ .(الأحمر–الميت) جفاف البحر الميت وقناة البحرين .IUG Journal of Natural Studies. 2015;15.(2)

46. Pletcher K. Dead Sea. Encyclopedia Britannica2022.

47. Al Bawab A, Bozeya A, Abu-Mallouh S, Daqour I, Abu-Zurayk RA ,editors. The Dead Sea mud and salt: A review of its characterization, contaminants, and beneficial effects. IOP conference series: materials science and engineering; 2018: IOP Publishing.

48. Tyler RH, Boyer TP, Minami T, Zweng MM, Reagan JR. Electrical conductivity of the global ocean. Earth, Planets and Space. 2017;69(1):1-10.

49. Somaraju R, Trumpf J. Frequency, temperature and salinity variation of the permittivity of seawater. IEEE transactions on Antennas and Propagation. 2006;54(11):3441-8.

50. Woodard J. What is TDS in Water & Why Should You Measure It? : Fresh water system; March 23, 2021 [Available from: https://www.freshwatersystems.com/blogs/blog/what-is-tds-in-water-why-should-you-measure-it.

51. Ishtaiwi M, Hajjyahya M, Habbash S. Electrical properties of dead sea water. Journal of Applied Mathematics and Physics. 2021;9(12):3094-101.

52. Choudhary YS, Jothi L, Nageswaran G. Chapter 2 - Electrochemical Characterization. In: Thomas S, Thomas R, Zachariah AK, Mishra RK, editors. Spectroscopic Methods for Nanomaterials Characterization: Elsevier; 2017. p. 19-54.

53. Yun C, Hwang S. Analysis of the charging current in cyclic voltammetry and supercapacitor's galvanostatic charging profile based on a constant-phase element. ACS omega. 2020;6.73-367:(1)

54. Hsia B. Materials synthesis and characterization for micro-supercapacitor applications: University of California, Berkeley; 2013.

55. Insight P. Specific capacitance from galvanostatic charge discharge curves | Energy density and power density.2020 .

56. Effendy S, Song J, Bazant MZ. Analysis, design, and generalization of electrochemical impedance spectroscopy (EIS) inversion algorithms. Journal of The Electrochemical Society. 2020;167(10):106508.

57. Canales P. C. Electrochemical Impedance Spectroscopy and Its Applications. 21st Century Nanostructured Materials—Physics, Chemistry, Classification, and Emerging Applications in Industry, Biomedicine, and Agriculture. 2021.

58. Syed K. Abbas, Anwar MS. Electrochemical Impedance Spectroscopy (EIS (Gamry Interface 1010E Potentiostat/Galvanostat/ZRA PHYSLAB. 2021.

59. Mei B-A, Munteshari O, Lau J, Dunn B, Pilon L. Physical interpretations of Nyquist plots for EDLC electrodes and devices. The Journal of Physical Chemistry C. 2018;122(1):194-206.

60. جرار، صبري ص. Carbon Nanofibers/Graphene Nanoplateletes Composite as Supercapacitor Electrode Using KOH Aqueous Electrolyte: An-Najah National University; 2020.

61. Bashir S, Iqbal J, Farhana K, Jafer R, Hina M, Kasi R, et al. Hybrid organic polymer electrolytes for dye-sensitized solar cells. Dye-Sensitized Solar Cells: Elsevier; 2022. p. 181-212.

62. Ma C, Yu Y, Li Y-j, Shi J-l, Song Y, Liu L. Ion accumulation and diffusion behavior in micro-/meso-pores of carbon nanofibers. Journal of The Electrochemical Society. 2014;161(9):A1330.

63. White CM, Smith DH, Jones KL, Goodman AL, Jikich SA, LaCount RB, et al. Sequestration of carbon dioxide in coal with enhanced coalbed methane recovery a review. Energy & Fuels. 2005;19(3):659-724.

64. Farrukh A. Brunauer–Emmett–Teller (BET) Adsorption Isotherm: Calculations for BET and Specific Surface Area In: farrukh aM, editor. Learning Physical Chemistry and Nano-Chemistry2021.

65. Lowell S, Shields JE, Thomas MA, Thommes M. Characterization of porous solids and powders: surface area, pore size and density: Springer Science & Business Media; 2006.

66. USP-NF. Specific Surface Area. Pharmacopeial Forum. 2004;30:1465 - 94.

67. Zhou X, Zhao T, An L, Zeng Y, Yan X. A vanadium redox flow battery model incorporating the effect of ion concentrations on ion mobility. Applied energy. 2015;158:157-66.

68. Chen Q, Ma J, Zhang Y, Wu C, Xu J. Effects of temperature and ionic concentration on nanodroplet electrocoalescence. Langmuir. 2018;35(3):750-9.

69. Stephen Lower, Kahlon A .The Hydronium Ion: Libretexts chemistry; 2022, Aug. 10 [Available from: https://chem.libretexts.org/Bookshelves/Physical_and_Theoretical_Chemistry_Textbook_Maps/Supplemental_Modules_(Physical_and_Theoretical_Chemistry)/Acids_and_Bases/Acids_and_Bases_in_Aqueous_Solutions/The_Hydronium_Ion.

70. Chowdhury A, Dhar A, Biswas S, Sharma V, Burada PS, Chandra A. Theoretical model for magnetic supercapacitors—From the electrode material to electrolyte ion dependence. The Journal of Physical Chemistry C. 2020;12.24-26613:(49)4

71. Cheng B, Cheng R, Tan F, Liu X, Huo J, Yue G. Highly efficient quasi-solid-state asymmetric supercapacitors based on MoS 2/MWCNT and PANI/MWCNT composite electrodes. Nanoscale Research Letters. 2019;14:1-12.

72. Yu J, Fu N, Zhao J, Liu R, Li F, Du Y, et al. High specific capacitance electrode material for supercapacitors based on resin-derived nitrogen-doped porous carbons. ACS omega. 2019;4(14):15904-11.

73. Layton BE. A comparison of energy densities of prevalent energy sources in units of joules per cubic meter. International Journal of Green Energy. 2008;5(6):438-55.

74. Oyedotun KO. Synthesis and characterization of carbon-based nanostructured material electrodes for designing novel hybrid supercapacitors: University of Pretoria.2018 ;

75. Yoon S-B, Jegal J-P, Roh KC, Kim K-B. Electrochemical impedance spectroscopic investigation of sodium ion diffusion in MnO2 using a constant phase element active in desired frequency ranges. Journal of The Electrochemical Society. 2014;161(4):H2.07

76. Laschuk NO, Easton EB, Zenkina OV. Reducing the resistance for the use of electrochemical impedance spectroscopy analysis in materials chemistry. RSC advances. 2021;11(45):27925-36.

77. Taberna P, Simon P, Fauvarque J-F. Electrochemical characteristics and impedance spectroscopy studies of carbon-carbon supercapacitors. Journal of the Electrochemical Society. 2003;150(3):A292.

78. Hussain S, Amade R, Jover E, Bertran E. Nitrogen plasma functionalization of carbon nanotubes for supercapacitor applications. Journal of Materials Science. 2013;48:7620-8.

Appendices

Appendix A

Figures

Figure 1.2

Simple scheme of the construction of supercapacitor

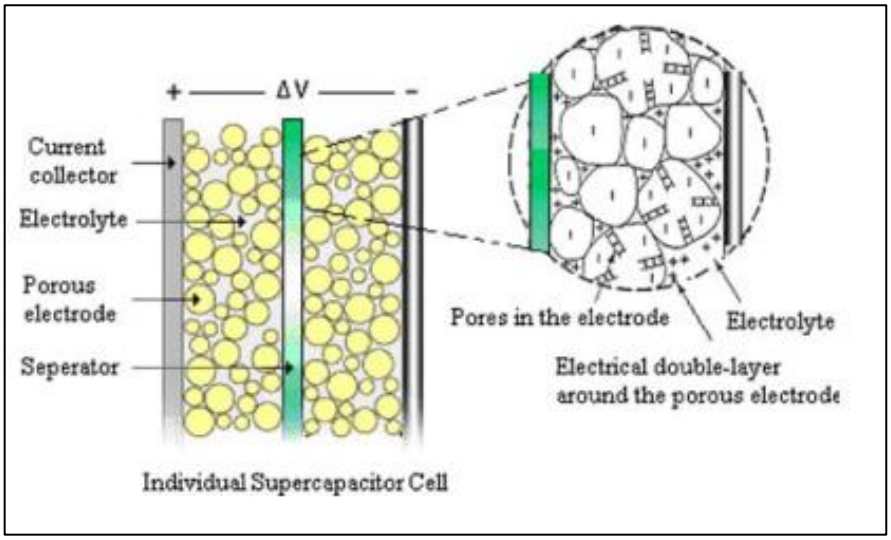

Note: Pan H, Li J, Feng Y.Carbon nanotubes for supercapacitor. Nanoscale research letters.2010;5:654-68.

Figure 1.3

Charging (b) and discharging (a) process in EDLC

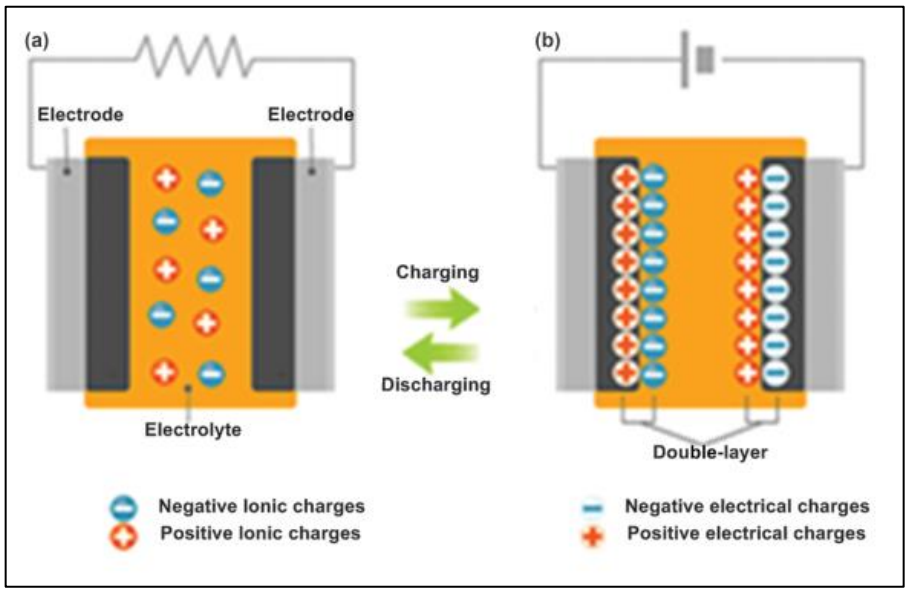

Note: Lourenço L, Branco PC. Electric Energy Storage using Ionic Polymer Metal Composites: Towards a Flexible Ionic Polymer Metal Composite Capacitor for Low-power Devices. Ionic Polymer Metal Composites (IPMCs)2015. p. 286-333.

Figure 1.4

Types of electrolytes typically used in supercapacitors

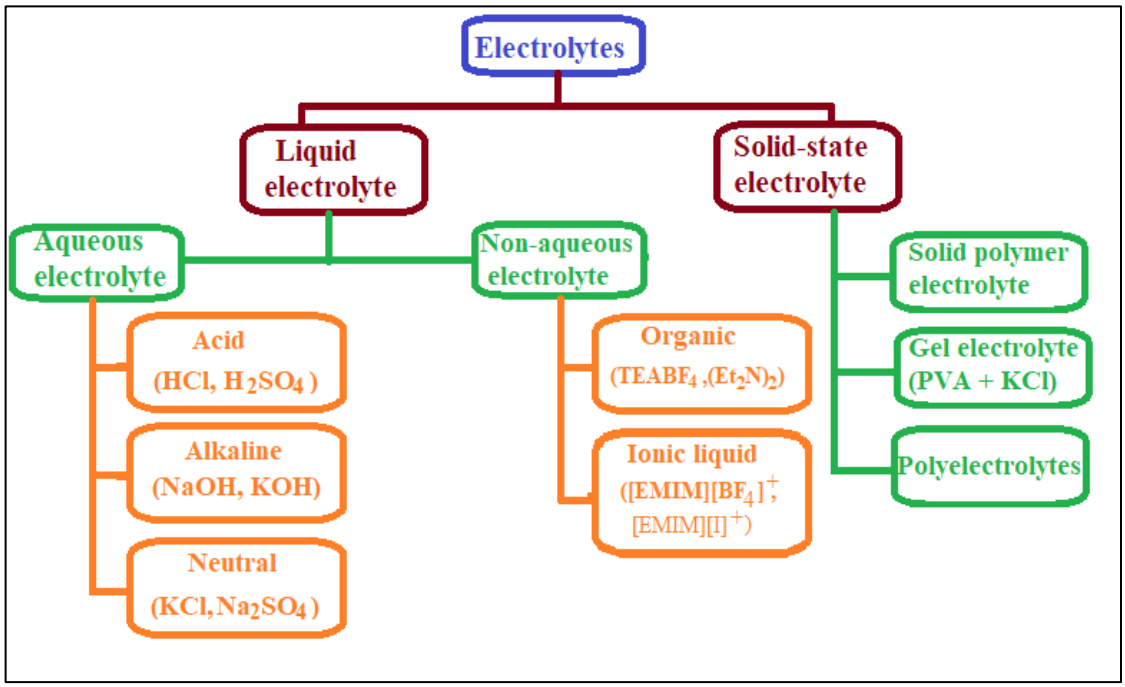

Note: Samsudin NA, Lim Y-C, Chang S-K, Heng I, Low FW, Shakeri M, et al. Titanium Dioxide Nanostructured Based Supercapacitors. 2022.

Figure 2.1

A diagram of supercapacitor illustrating energy storage in electric double layers at electrode-electrolyte interfaces

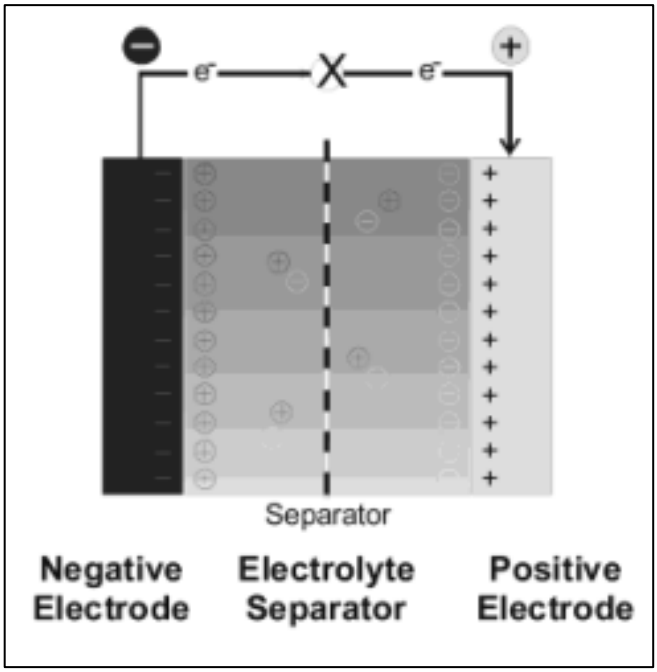

Note: Winter M, Brodd RJ. What Are Batteries, Fuel Cells, and Supercapacitors? Chemical Reviews. 2004;104(10):4245-70.

Figure 2.2

Classification of the different types of supercapacitors

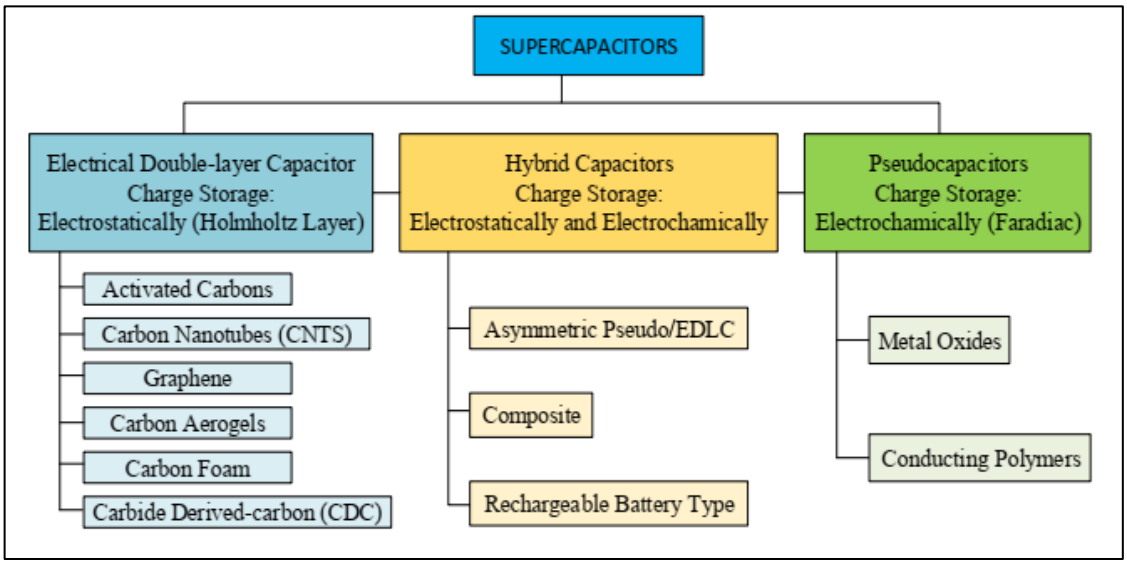

Note: Sahin ME, Blaabjerg F, Sangwongwanich A. A review on supercapacitor materials and developments. Turkish Journal of Materials. 2020;5(2):10-24.

Figure 2.3

Scheme of supercapacitors

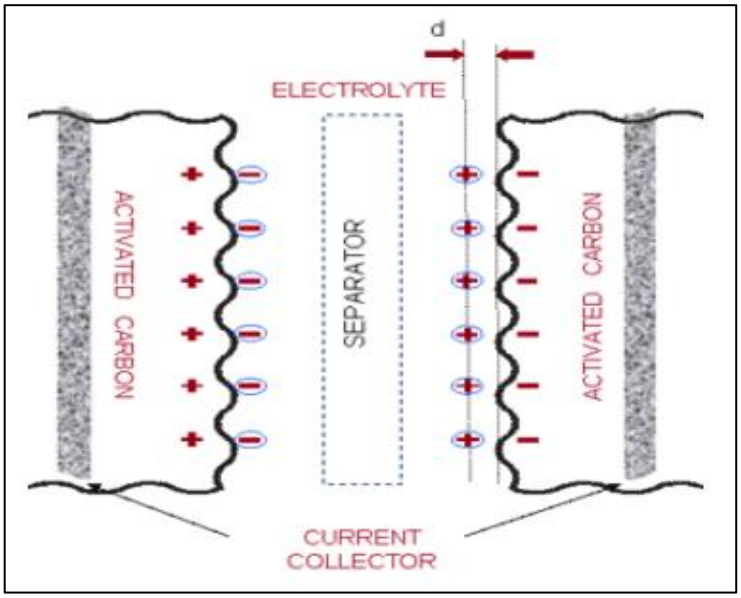

Note: Gidwani M, Bhagwani A, Rohra N. Supercapacitors: the near future of batteries. International Journal of Engineering Inventions. 2014;4(5):22-7.

Figure 2.4

Scheme of electrostatic capacitor

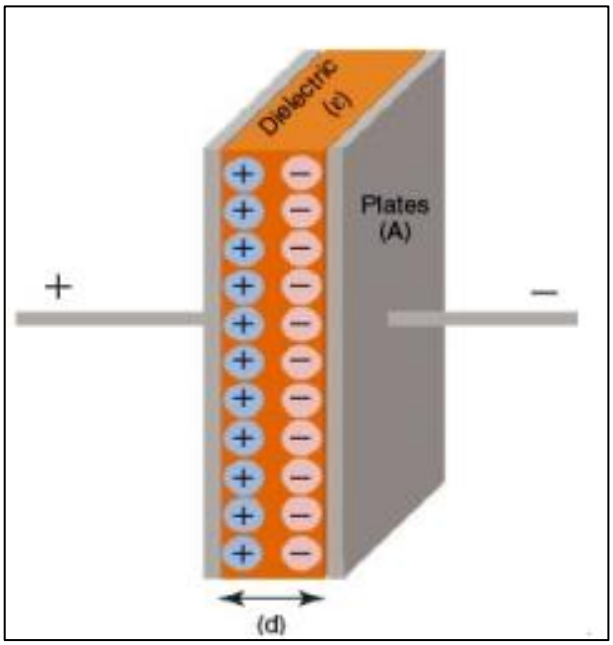

Note: Sahin ME, Blaabjerg F, Sangwongwanich A. A review on supercapacitor materials and developments. Turkish Journal of Materials. 2020;5(2):10-24.

Figure 2.5

Drift of charges in supercapacitor

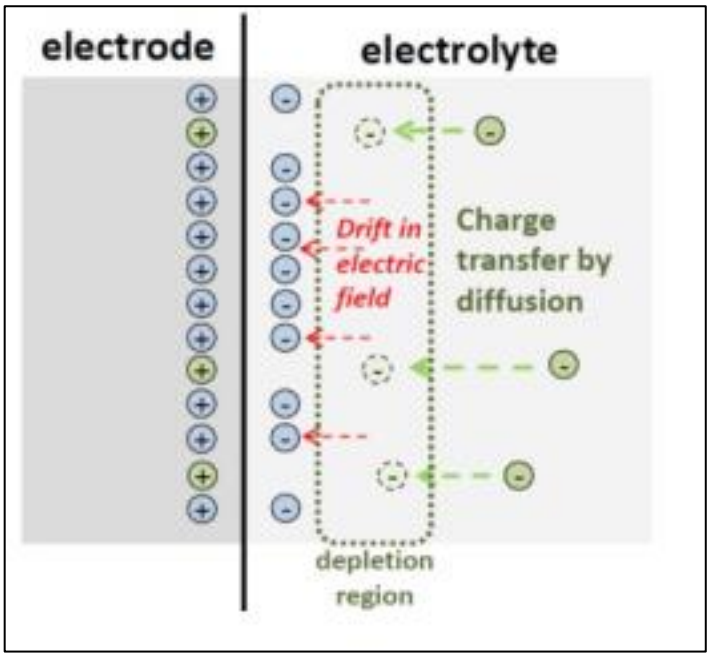

Note: Sahin ME, Blaabjerg F, Sangwongwanich A. A review on supercapacitor materials and developments. Turkish Journal of Materials. 2020;5(2):10-24.

Figure 2.6

The eight forms of carbon allotropes

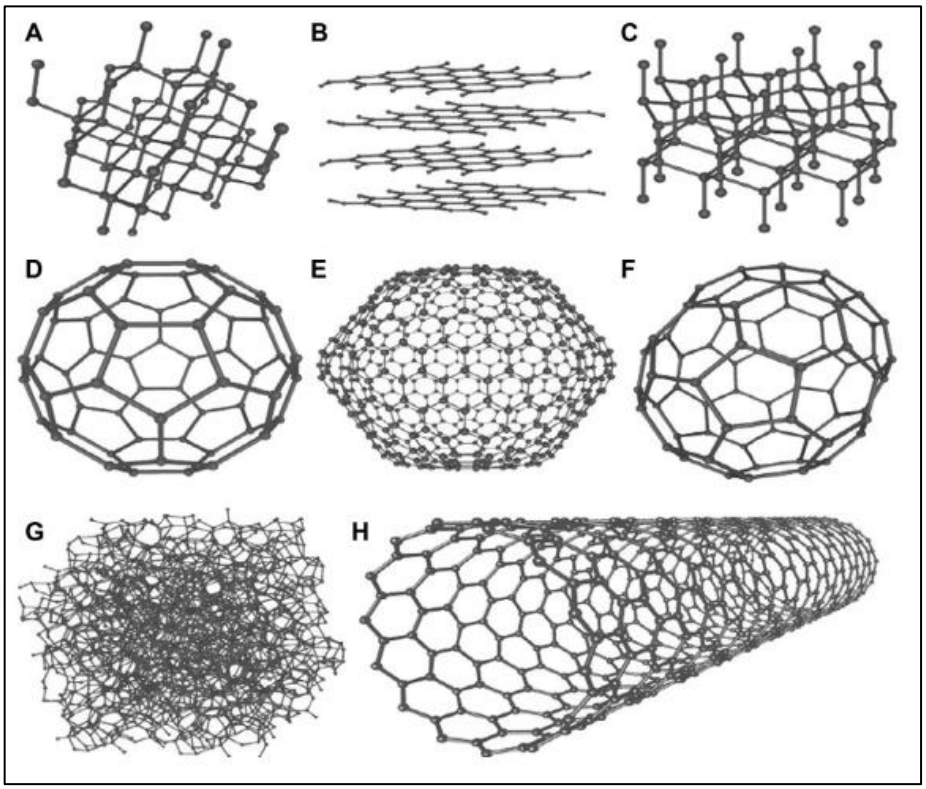

Note: Aqel A, Abou El-Nour KM, Ammar RA, Al-Warthan A. Carbon nanotubes, science and technology part (I) structure, synthesis and characterisation. Arabian Journal of Chemistry. 2012;5(1):1-23.

Figure 2.7

Illustrations represent different shapes of carbon nanofibers

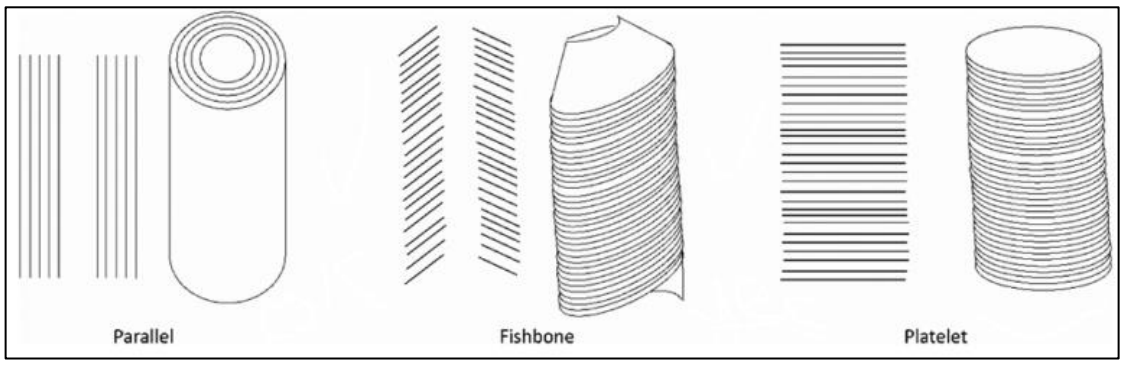

Note: Ruiz-Cornejo JC, Sebastián D, Lázaro MJ. Synthesis and applications of carbon nanofibers: a review . Reviews in Chemical Engineering. 2020;36(4):493-511

Figure 2.8

The cyclic voltammogram shows the redox peaks

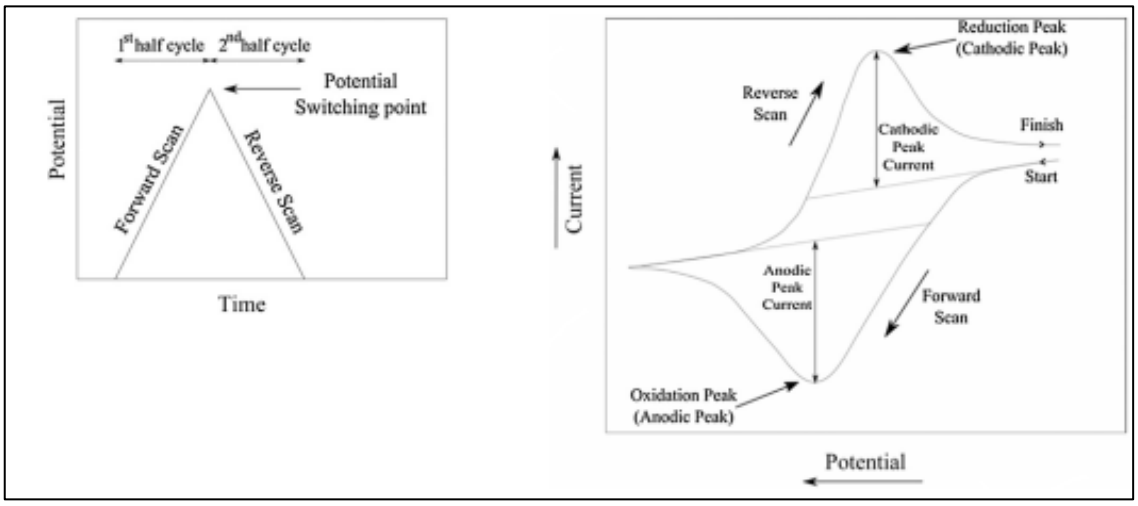

Note: Choudhary YS, Jothi L, Nageswaran G. Chapter 2 - Electrochemical Characterization. In: Thomas S, Thomas R, Zachariah AK, Mishra RK, editors. Spectroscopic Methods for Nanomaterials Characterization: Elsevier; 2017. p. 19-54.

Figure 2.9

Some common GCD plots; a) an ideal charge/discharge cycle with the indicated slope; b) a charging curve that exceeds the electrolyte stability window, resulting in excess charge transfer; and c) a discharge curve preceded by a significant IR potential drop

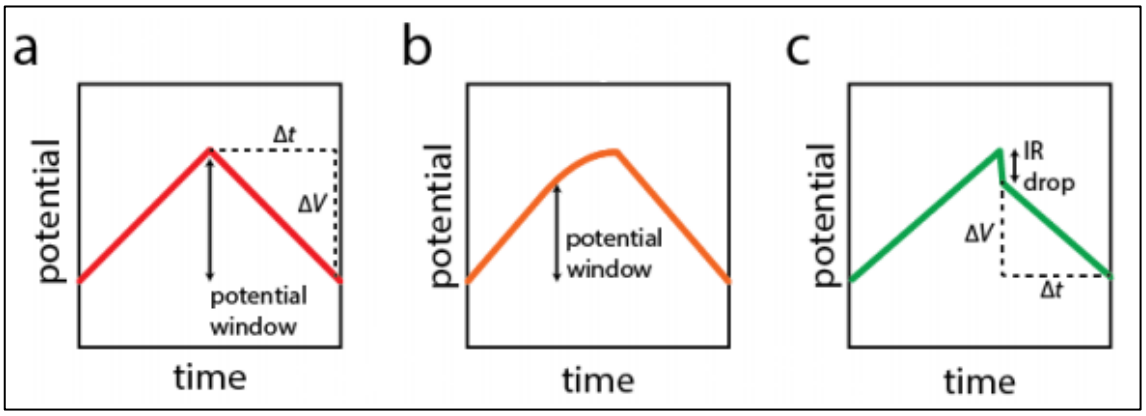

Note: Hsia B. Materials synthesis and characterization for micro-supercapacitor applications: University of California, Berkeley; 2013.

Figure 2.10

Nyquist plot components

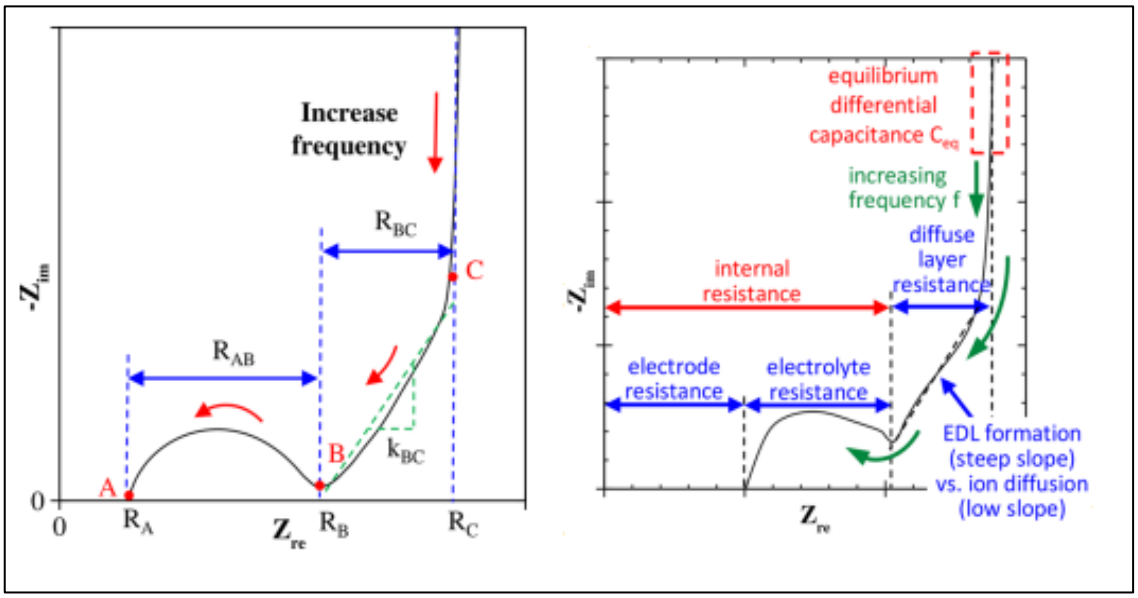

Note: Mei B-A, Munteshari O, Lau J, Dunn B, Pilon L. Physical interpretations of Nyquist plots for EDLC electrodes and devices. The Journal of Physical Chemistry C. 2018;122(1):194-206

Figure 2.11

The fundamental types of physical adsorption isotherms

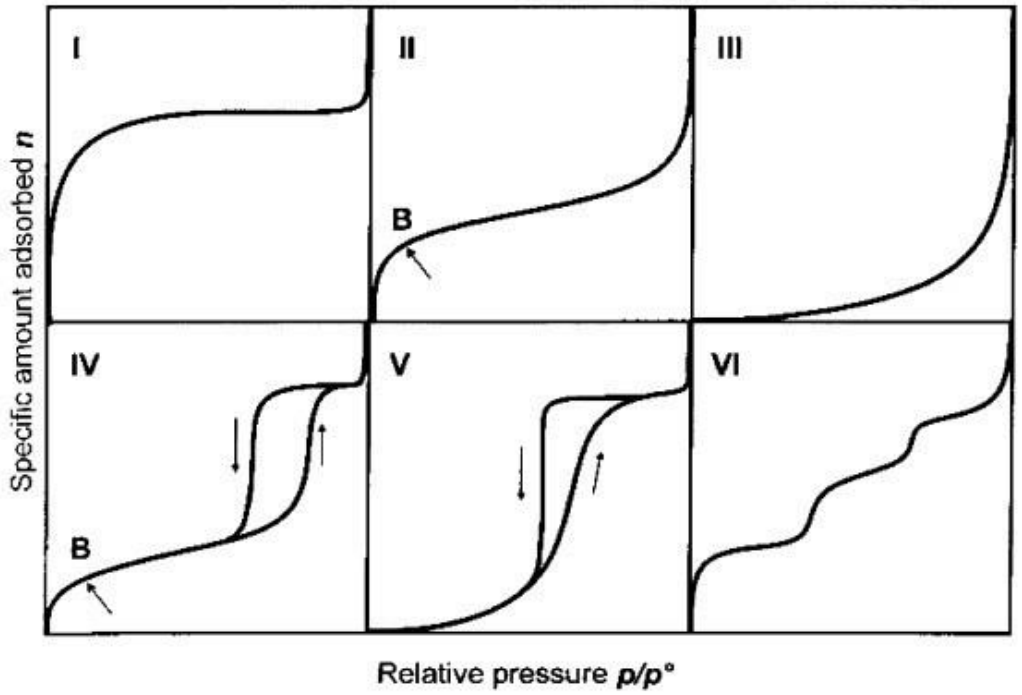

Note: White CM, Smith DH, Jones KL, Goodman AL, Jikich SA, LaCount RB, et al. Sequestration of carbon dioxide in coal with enhanced coalbed methane recovery a review. Energy & Fuels. 2005;19(3):659-724.

Figure 2.12

Typical BET plot

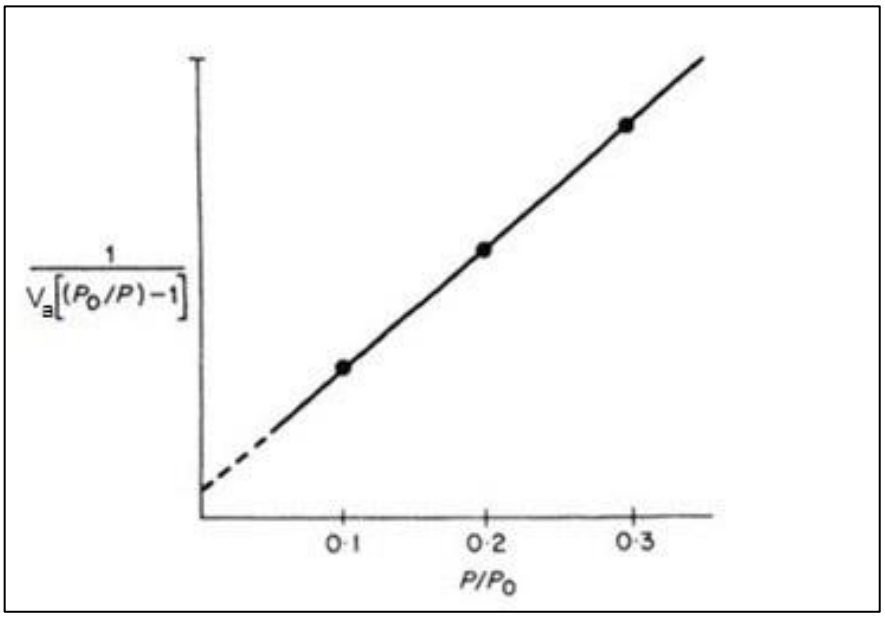

Note: Lowell S, Shields JE, Thomas MA, Thommes M. Characterization of porous solids and powders: surface area, pore size and density: Springer Science & Business Media; 2006.

Figure 4.10

Cyclic stability for AC/CNFs electrodes using different electrolytes at current = 100 mA

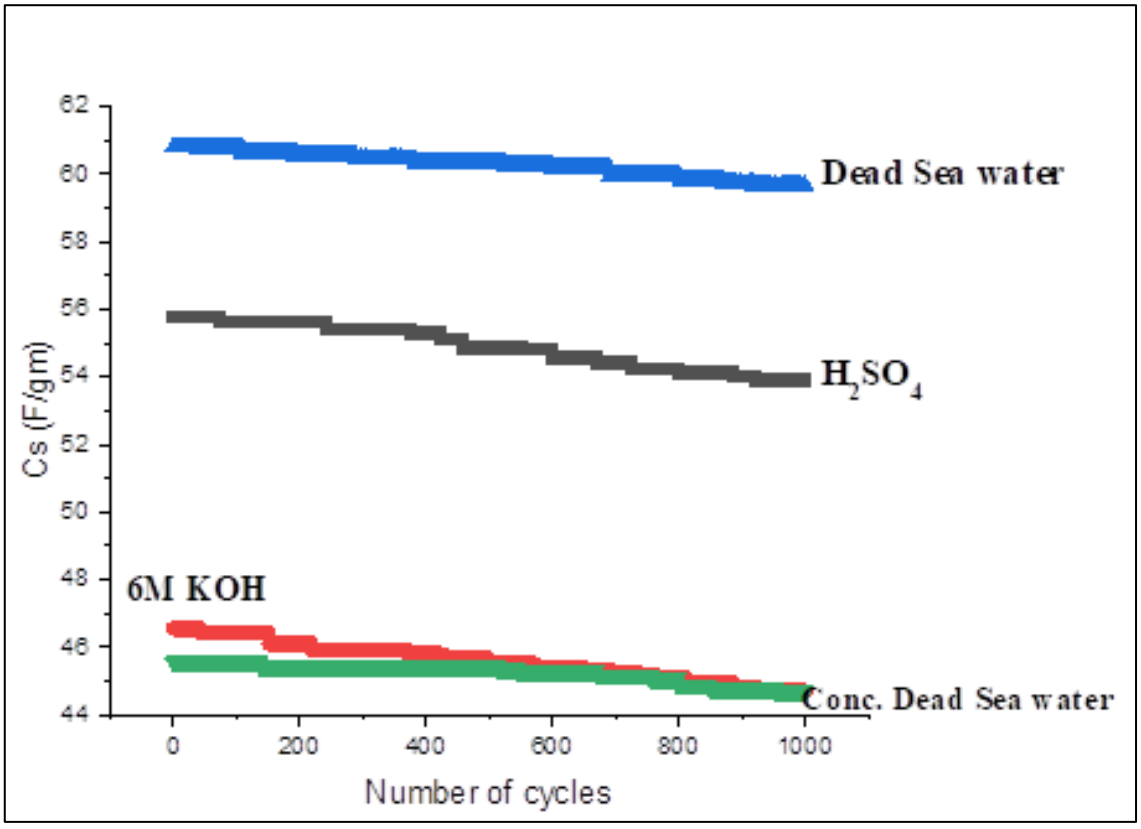

Figure 4.11

Nyquist plot from electrochemical impedance spectroscopy for AC/CNFs electrodes in different electrolytes.

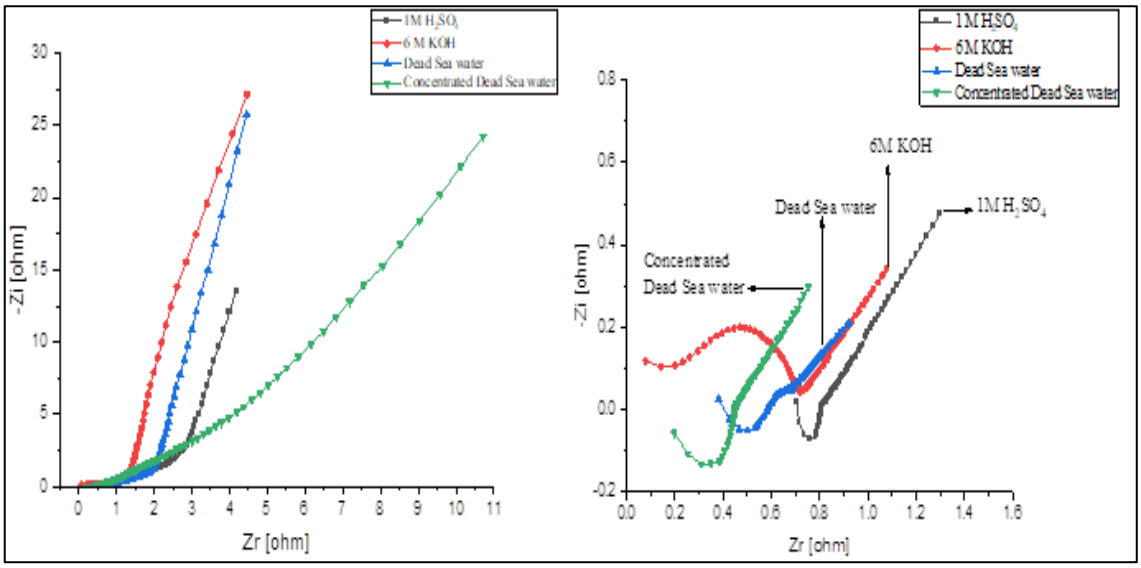

Figure 4.12

Specific capacitance relation with frequency for all used electrolytes

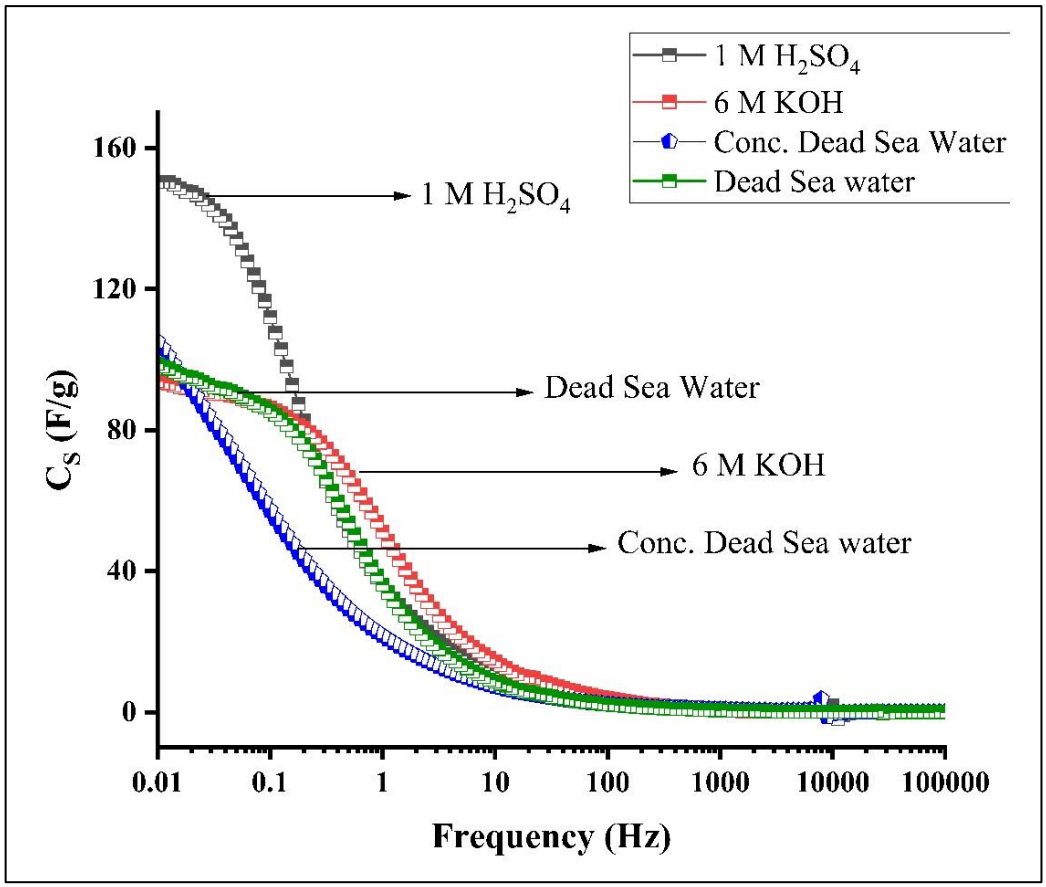

Figure 4.13

The relationship between the real part of the impedance (Zr) vs. frequency

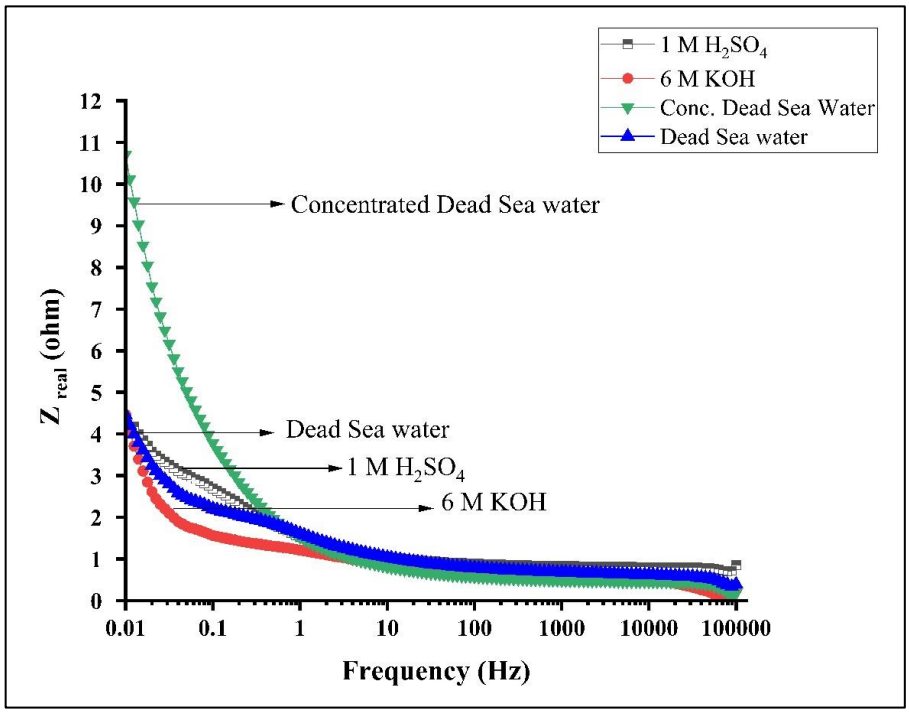

Figure 4.14

The relationship between the imaginary part of the impedance (Zi) vs. frequency

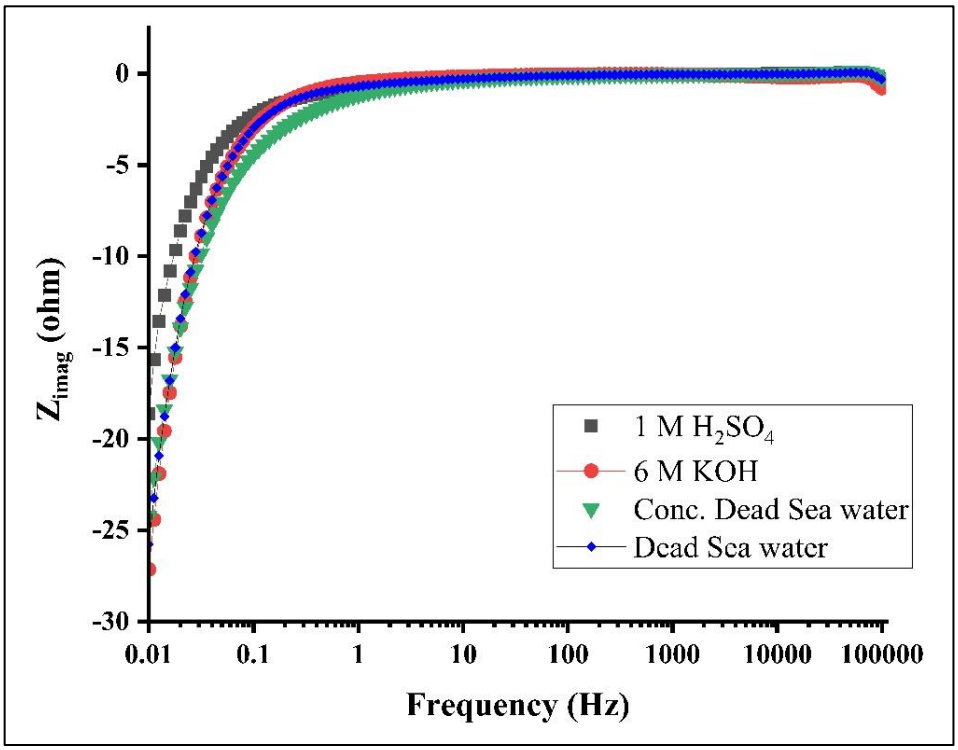

Figure 4.15

The relationship between the imaginary component of the capacitance (C") vs. frequency

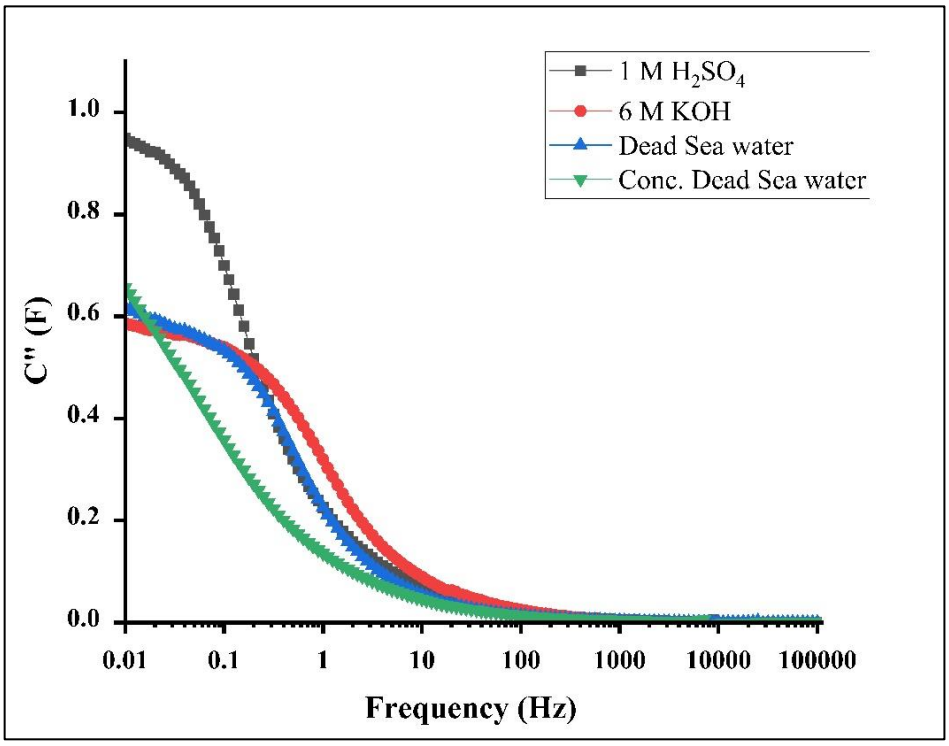

Figure 4.16

EIS phase angle comparison across all samples as a function of frequency logarithm (Bode plot)

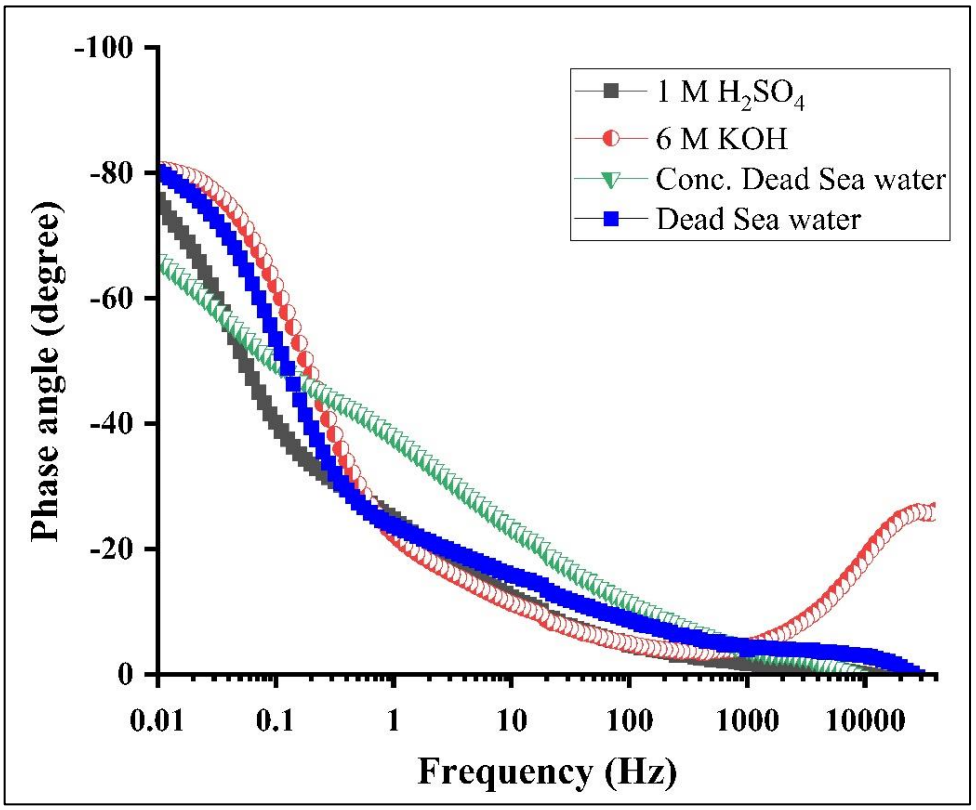

Figure 4.17

SEM images

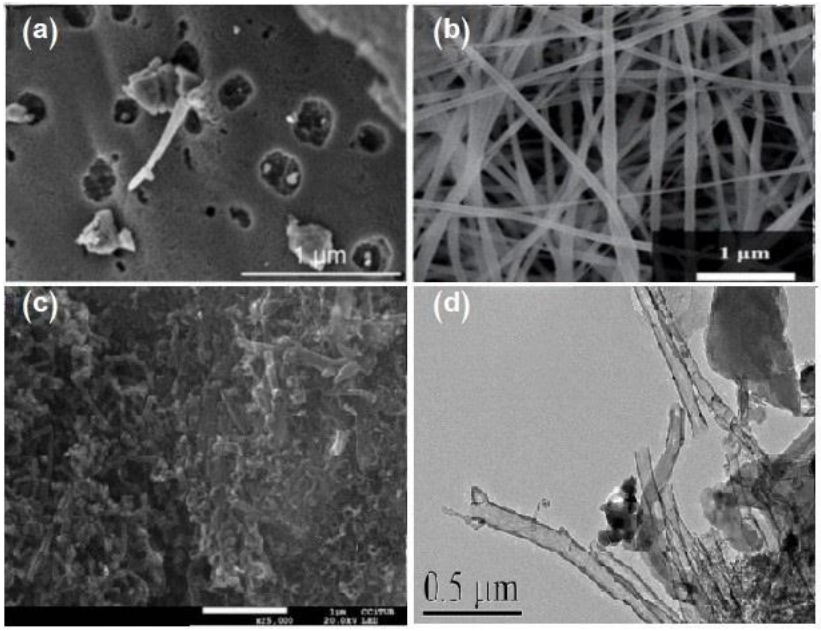

a) activated carbon (AC), b) carbon nanofibers (CNFs), c) a prepared electrode of AC (90 wt%) and CNFs (10 wt%) hydraulically pressed at 8 tons , and d) TEM image of sample (90% AC / 10 % CNFs)

Note: Daragmeh A .Advances in carbon nanofiber-based supercapacitors. 2017.

Figure 4.18

The N_2 adsorption /desorption isotherm for AC/CNFs composite electrode

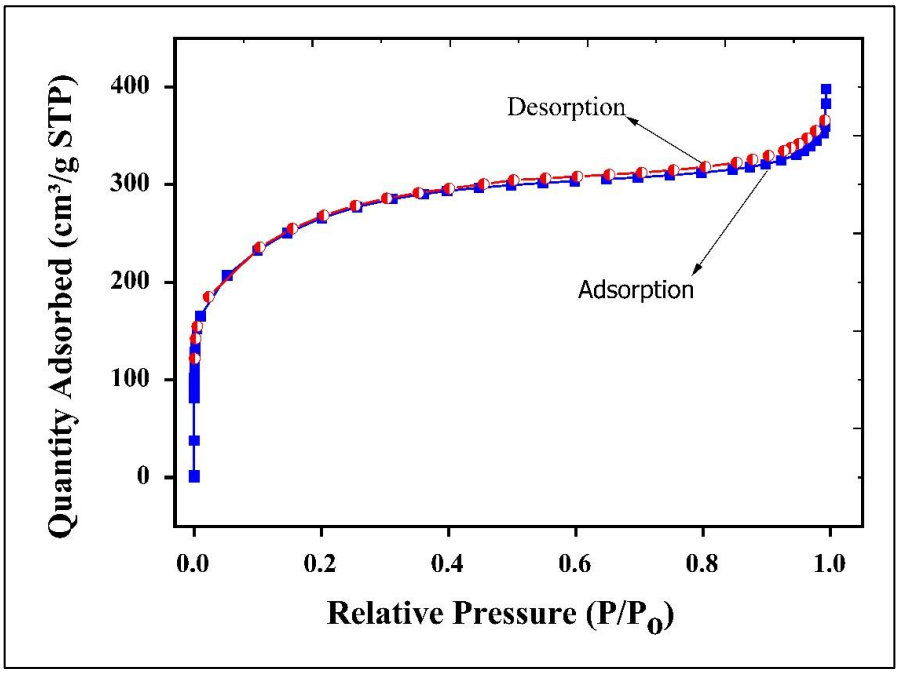

Figure 4.19

Linear BET plot for AC/CNFs composite electrode

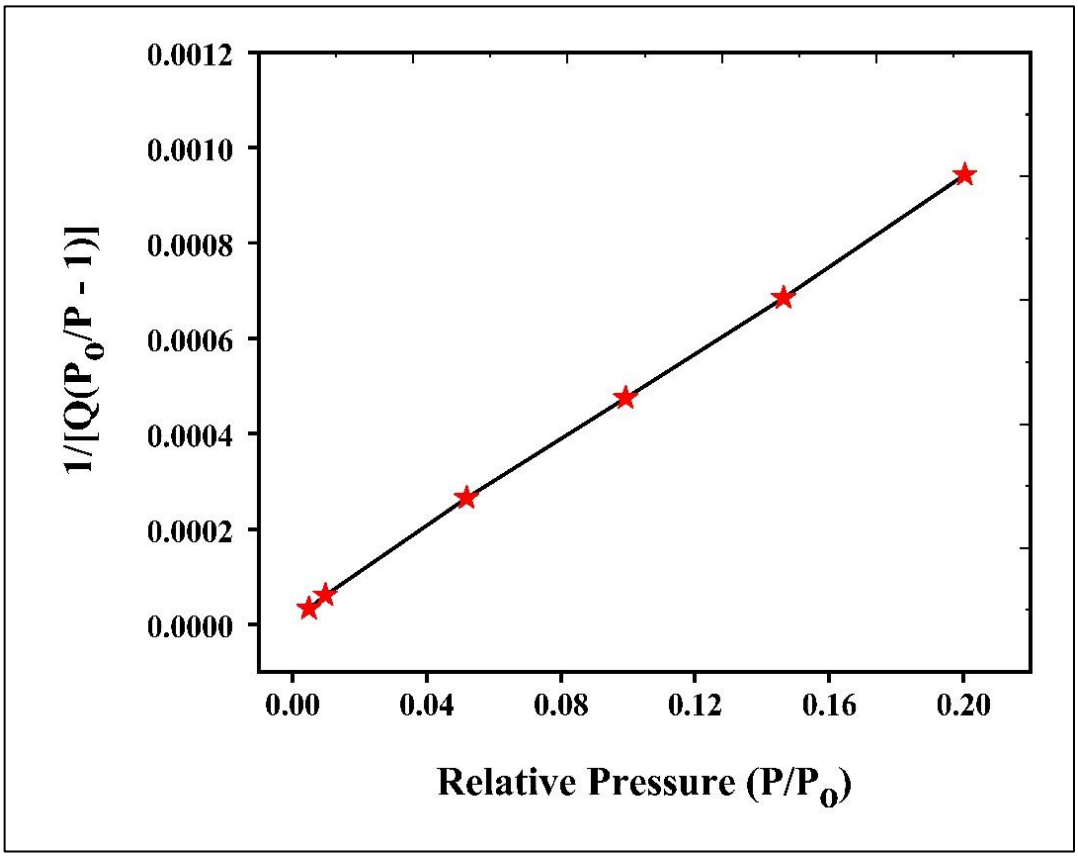

Appendix B

Tables

Table 4.6

Power and Energy densities for AC/CNFs electrodes using different electrolytes

Current (A)	1 M H_2SO_4		6 M KOH		Dead Sea water		Concentrated Dead Sea water	
	E_d (Wh/Kg)	P_d (W/Kg)	E_d (Wh/Kg)	P_d (W/Kg)	E_d (Wh/Kg)	P_d (W/Kg)	E_d (Wh/Kg)	P_d (W/Kg)
0.01	10.535	385.43	6.897	428.1	10.157	376.94	10.213	372.88
0.02	9.595	746.08	6.725	754.23	8.658	723.16	7.845	714.98
0.04	8.079	1420.96	6.25	1472.61	6.964	1347.27	5.536	1280.77
0.05	7.145	1696.86	5.638	1734.91	6.0145	1608.65	4.497	1471.77
0.07	5.706	2199.37	4.967	2365.36	4.825	2048.44	3.145	1736.37
0.10	3.937	2829.01	3.924	3071.14	3.442	2473.84	1.657	1968.67
0.15	1.922	3460.33	2.520	3780.66	1.262	2263.71	0.478	1704.37

Table 4.10

The phase angle for the prepared supercapacitors using different electrolytes

Sample	Phase angle
1 M H_2SO_4	-72.9°
6 M KOH	-80.7°
Dead Sea water	-83.6°
Concentrated Dead Sea water	-66.2°

Table 4.11

The calculated specific surface area and total volume depend on the analysis of the linear BET plot for the AC/CNFs composite electrode

Slope (s) (g/cm^3 STP)	Y-intercept (i) (g/cm^3 STP)	V_m (cm^3/g STP)	Sample mass (g)	S_{BET} m^2/g	V_{total} cm^3/g
0.004512	0.000013	221.0	0.4991	962.06	0.693

جـامعـــة النجاح الوطنية
كليـــة الدراســـات العليـــا

دراسة الكربون النشط / ألياف الكربون النانوية كأقطاب كهربائية فائقة السعة باستخدام محاليل كهرلية مائية مختلفة (حمض الكبريتيك وهيدروكسيد الصوديوم وتركيز مختلفة من مياه البحر الميت)

إعداد
خلود وليد بوريني

إشراف
د. علان دراغمة
د. إياد سعد الدين

قُدّمت هذه الرسالة استكمالا لمتطلبات الحصول على درجة الماجستير في الفيزياء من كلية الدراسات العليا في جامعة النجاح الوطنية، نابلس- فلسطين.

2024

دراسة الكربون النشط / ألياف الكربون النانوية كأقطاب كهربائية فائقة السعة باستخدام محاليل كهرلية مائية مختلفة (حمض الكبريتيك وهيدروكسيد الصوديوم وتركيز مختلفة من مياه البحر الميت)

إعداد

خلود وليد بوريني

إشراف

د. علان دراغمة

د. إياد سعد الدين

الملخص

في هذه الرسالة يتم دراسة تأثير أنواع مختلفة من المحاليل الكهرلية المائية على الخصائص الكهروكيميائية للقطب الكهربائي المركب من الكربون المنشط وألياف النانو الكربونية (AC%90) و (CNFs %10) في المكثفات الفائقة. استخدمت المحاليل الكهرلية: ($1M\ H_2SO_4$) و(6 M KOH)، ومياه البحر الميت، ومياه البحر الميت المركزة. تم إجراء التجارب باستخدام تقنيات قياس الجهد الحلقي (CV)، الشحن والتفريغ الجلفانوستاتي (GCD)، والتحليل الطيفي للمعاوقة الكهروكيميائية (EIS). استُخدمت تقنية الجهد الحلقي بمعدل مسح 100 ملي فولت/ثانية لتقييم أداء الأقطاب الكهربائية. أظهرت الأقطاب الكهربائية مع محاليل M (H_2SO_4) و(6 M KOH) ومياه البحر الميت سعات نوعية متقاربة تصل إلى (78.50، 77.40، و78.54) فراد/غم على التوالي، بينما سجل القطب مع مياه البحر الميت المركزة أدنى سعة بمقدار 56.54 فراد/غم. عند تخفيض معدل المسح إلى (5) ملي فولت/ثانية، سجل القطب مع (6 M KOH) أعلى سعة نوعية (157.86 فراد/غم)، بينما كانت الأقطاب مع المحاليل الأخرى تتراوح سعاتها بين (134.30 و145.46) فراد/غم.

وُجد أن السعة النوعية للمكثفات الفائقة تنخفض مع زيادة كثافة التيار. أظهر المكثف مع محلول مياه البحر الميت المركزة أعلى سعة عند كثافة تيار منخفضة (0.4) أمبير/غم بقيمة (84.40) فراد/غم، في حين كانت سعة المكثف مع (6 M KOH) الأقل بمقدار (52.40) فراد/غم.

تم تقييم المعاوقة الكهروكيميائية لكل خلية بتعريضـها لموجة جيبية بجهد 20 ميلي فولت عبر نطاق ترددي من 10 ميلي هرتز إلى 100 كيلوهرتز. كشفت النتائج عن أقصى سعات لقطب AC/CNFs مع محاليل ($1\ M\ H_2SO_4$) ومياه البحر الميت المركزة ومياه البحر الميت و($6\ M\ KOH$) بقيم 150.3، 105.1، 98.8 و93.8 فراد/غم على التوالي. أظهر القطب مع مياه البحر الميت المركزة أعلى تردد ركبة 0.125 هرتز، ما يعد مثاليًا للمكثفات الفائقة.

بالنسبة لمورفولوجيا سطح القطب الكهربائي، تبين أن السطح خشن ومسامي مع مساحة سطحية كبيرة (962.06 $م^2$/غرام) وحجم مسام صغير (0.693 $سم^3$/غرام)، ما يعكس السلوك الكهربائي المرغوب فيه للمكثفات الفائقة.

الكلمات المفتاحية: الكربون النشط (AC)، ألياف الكربون النانوية (CNFs)، أقطاب المكثفات الفائقة، الشوارد المائية، مياه البحر الميت.